FINITE ELEMENT STRESS ANALYSIS AND EXPERIMENTAL VERIFICATION FOR DYNAMIC LOADING OF TWO MODELS OF THREE WHEELER VIKRAM CHASSIS FRAME

by

SANDEEP MEHROTRA

DEPARTMENT OF MECHANICAL ENGINEERING

INDIAN INSTITUTE OF TECHNOLOGY KANPUR

FEBRUARY 1997

FINITE ELEMENT STRESS ANALYSIS AND EXPERIMENTAL VERIFICATION FOR DYNAMIC LOADING OF TWO MODELS OF THREE WHEELER VIKRAM CHASSIS FRAME

A thesis submitted in
Partial Fulfillment of the Requirements
for the degree of
MASTER OF TECHNOLOGY
in
MECHANICAL ENGINEERING

by
SANDEEP MEHROTRA

to the
DEPARTMENT OF MECHANICAL ENGINEERING
INDIAN INSTITUTE OF TECHNOLOGY, KANPUR
February, 1997

ME-1987-M-MEH-FIN.

CERTIFICATE

This is to certify that the work contained in this thesis, entitled **"Finite Element Stress Analysis and Experimental Verification for Dynamic Loading of two models of Three Wheeler Vikram Chassis Frame"**, by Sandeep Mehrotra, has been carried out under my supervision. This work has not been submitted elsewhere for a degree.

Dr. B. Sahay

Professor and Head

Department of Mechanical Engineering

Indian Institute of Technology

Kanpur - 208016

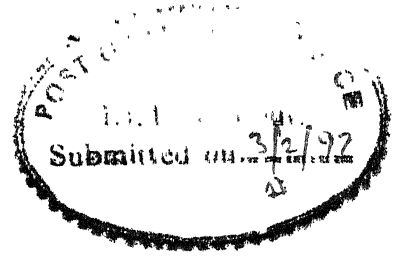

ABSTRACT

This work finds out the stresses developed in the critical sections of the two models of the three wheelers Vikram chassis frame at selected cross sections. Computer modeling of the two chassis has been done. Using this computer model finite element analysis of the two chassis has been undertaken to determine and compare the stresses developed in them at critical sections. Analysis has been done for three different dynamic loading conditions. For one loading condition experimental stress analysis at some selected points has been performed to verify the FEA model and results for both the models.

ACKNOWLEDGMENT

I express my deep sense of gratitude and indebtedness to my thesis supervisor Dr. B. Sahay for his invaluable guidance and constant encouragement through out the present work. I am thankful to Dr. N.N. Kishore for helping me in doing the computer modeling for NISA. I am equally thankful to Dr. P. Kumar for giving me suggestions for performing experimental work and lending me his invaluable instruments for the doing experiments My sincere thanks to Dr. S.G. Dhande and to Dr. N. Vyas for constant encouragement through out this work.

I am also grateful to Dr. Sahay, CMD, and Mr A. Kumar, Manager, design and development, Scooters India Ltd., Lucknow, for their help rendered during the course of this project and also making two models of Vikram available for experimentation. My sincere thanks to Mr. Sarkar, Mr. Singh, Mr. Srivastava and Mr. Verma for their cooperation and valuable suggestions.

My sincere thanks to Mr. A. Ramakrishna for helping me with my experimentation on the vehicle. I am grateful to all my friends in CAD lab., Vibration lab. and E.S.A lab. for their help and friendly environment given to me during my work.

Sandeep Mehrotra

CONTENTS

LIST OF FIGURES

LIST OF TABLES

CHAPTER - 1

INTRODUCTION

1.1 PROBLEM DEFINITION

Three wheelers are popular city transport vehicles specially for short hauls of passengers and loads. One such three wheeler "VIKRAM" is manufactured by Scooters India Limited, Lucknow. This three wheeler has a major share of market in U.P..

Vikram was initially imported from an Italian company - Innocenti. This vehicle was designed with a two-stroke petrol engine. To make it suitable to the Indian requirements, the manufacturer in India has modified it by (a) replacing petrol engine with a diesel engine and (b) by increasing the length of the chassis.

The initial two stroke petrol engine of the three wheeler Vikram was very small in size, half the weight of the diesel engine now being used and it ran at much higher engine speeds as compared to the present one. Being a two stroke engine it had lesser unbalanced forces. The present engine is single cylinder four-stroke diesel engine primarily designed for stationary agricultural needs such as pumping water, running the thrashers etc. Because the engine has been designed to be anchored at one place and not for a vehicle, the unbalance forces are considerable along with the high noise level. Added to it are the bad road conditions, rash driving, and overloading due to which large forces are transferred through the road to the chassis frame.

Fig. 1.1 Top view of three wheeler Vikram (Side mounting)

Fig. 1.2 Front view of three wheeler Vikram (Side mounting)

Fig. 1.3 Top view of three wheeler Vikram (Central mounting)

Fig. 1.4 Front view of three wheeler Vikram (Central mounting)

Fig. 1.5 Three wheeler Vikram diesel engine

Due to dynamic forces and static loads, failure has been reported at three different sections of the chassis during the guaranty period of the vehicle. To over come this problem, the manufacturer has redesigned the old chassis. In the new design, the engine has been located in the middle of the chassis instead of the side. With the changed engine location, they have also changed the load carrying members. Since these changes have been incorporated very recently the manufacturer has no feed back concerning the new design.

Thus, the problem concerns the following:

(a) Computer modeling of the two chassis (with the old and new designs) acted upon by dynamic and static loads.

(b) Finite Element Analysis (FEA) of the two chassis models to determine and compare stresses at critical sections under the loading conditions.

(c) Experimental stress analysis at some critical sections verifying the FEA model and results.

1.2 LITERATURE SURVEY

In the moving automobile, different loads act on its parts and units. The magnitude and nature of these loads depends on wheel-road interaction, driver's action on controls, engine operating conditions and other factors. The reliability of an automobile depends on actual loads that act on it when in use. The automobile is the most complex object for determining load conditions, as its service conditions are very diverse and vary with time. Variable factors combine differently; the magnitude of stresses and the nature of their distribution in different parts vary within wide limits.

The forces causing these stresses may be constant (such as weight, forces which appear when the parts are tightened at the time of assembly, and the like) or variable (starting and braking forces. forces caused by manufacturing inaccuracies, road and operating conditions, resistance forces, dynamic forces, and others). Two types of strengths are recognized: static and fatigue strength. Static strength is the ability of a part to resist failure under the action of short time maximum loads. Fatigue strength is the ability of a part to resist failure under the action of repeatedly occurring loads, continuously varying or cumulative.

Since long, designers have been trying to design the automobile to make it for smoother ride, more comfortable, safer and stronger. Costin and Phipps [2] have tried to do chassis frame's stress calculation using force equilibrium method. They have found out the stresses developed in the different loads carrying members of their racing car for the static case.

Ali and Hedge [1] have done a FEM idealization of truck chassis frame and used it to predict deflections under various types of loads. They have also built a test rig to support the chassis frame to find out the deflections of the frame relative to a specially supported reference frame for out of plane bending, torsion and lateral loadings.

Sharman [8] has performed an experiment in which he recorded the strains at critical points on the chassis of a 16 ton GVW semi-trailer, operating on various road surfaces. He has used the statistical analysis of the records in terms of design factors and load spectra to determine the maximum static loads and have estimated the fatigue life.

Generally, the automobile industry have made various efforts for the better design of a chassis frame, no such data is available with the manufacturer of the particular three wheeler Vikram. The only work available on the three wheeler Vikram is done by Joshi [3]. For three wheeler Vikram's Side mounting frame, he has tried to bring out an improved design of the engine-mounting system which encounters least number of resonating phases during operation and thus looks for a design that results in less breakage of the exhaust pipe.

1.3 THE PRESENT WORK

The present work aims at predicting the behavior of the strength of the critical sections at the selected cross sections (node points) for both the models by doing finite element analysis for the following three different cases:

CASE I: When the engine is idling and vehicle is stationary.

CASE II: When the vehicle is running at 40 km./hr. in the fourth gear and its front wheel goes into a ditch of shape of half sine wave of 2 m wave length and 150 mm amplitude.

CASE III: When the vehicle is running at 40 km./hr. in the fourth gear and its both the rear wheels go into a ditch of shape of half sine wave of 2m wave length and 150 mm amplitude.

This work gives time Vs factor of safety plots for these selected points using maximum shearing stress theory. It compares two models at the critical sections for their strengths for all the three

cases. It also verifies the finite element model and results by experimental analysis on the selected points, for case I, for both the models.

Chapter 2 deals with the Finite element method formulation and those features of NISA related to the present work. The geometric modeling of the two types of chassis frames has been done in chapter 3 for pre-processing with NISA. The analysis results from the modeling are stated and discussed in Chapter 4. Experimental details and observations for the chassis frames are given in chapter 5. Finally, chapter 6 recommends the scope for further work that can be undertaken on the vehicle.

CHAPTER - 2

NISA - AN OVERVIEW

2.1 FINITE ELEMENT METHOD - A DEFINITION

Finite element method [10]is a powerful numerical technique for approximate solution of continuum mechanics and can be regarded as an extension of the Rayleigh-Ritz Procedure where piece-wise continuous trial functions are used. The method is approximate, since a continuum with infinite numbers of degrees of freedom is replaced with a discrete system with finite number of degrees of freedom. The method involves subdividing a continuum into a finite number of regions called elements connected at finite numbers of points called nodes to which loads are applied. An approximate admissible solution is constructed over the assemblage of elements, and the solution continuity is maintained at the inter-element boundaries.

2.2 NISA

NISA(Numerically Integrated elements for System Analysis) is a general purpose finite element program developed and maintained by EMRC to analyze a wide spectrum of problems encountered in engineering mechanics.

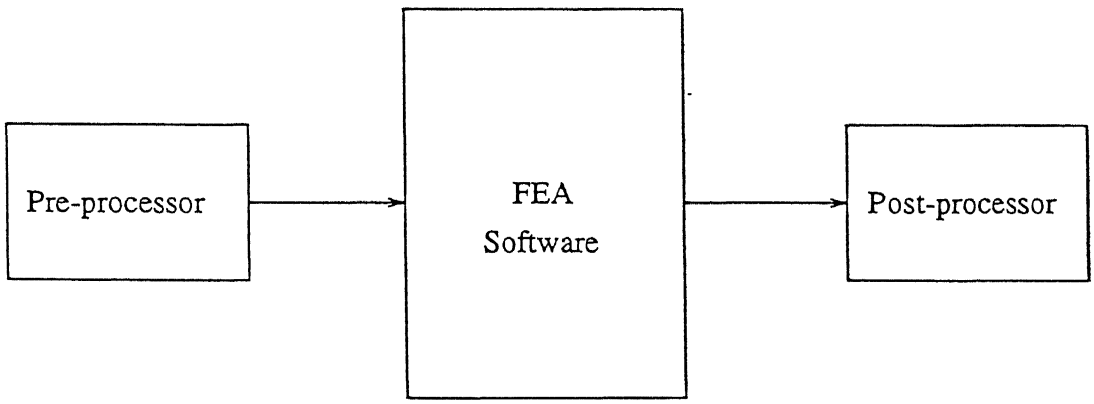

Fig. 2.1 Basic elements of a FEA software

2.2.1 GOVERNING EQUATION OF MOTION

The equations of motion describing the dynamic behavior of a structural system may be obtained from the extended Hamilton's principle for elastodynamics as:

$$\delta \int_{t_0}^{t_f} (U - T)dt - \int_{t_0}^{t_f} \delta W dt = 0 \tag{2.1}$$

where

δ = first variation

t_0, t_f = two arbitrary time points at which the first variation vanishes

U= strain energy in terms of geometrically compatible displacements

T= kinetic energy in terms of geometrically compatible displacements

δ W= virtual work of the external forces acting on the system during virtual displacements

The external forces may be conservative or nonconservative. A force is said to be conservative when its components are derivable from a potential function Nonconcervative forces, e.g. damping and follower forces, are deformation dependent, their magnitude and/or direction depend on the deformation. During the virtual displacements, the variations of the nonconservative forces are ignored. The virtual work δ W, therefore ,can be written as:

$$\delta W = -\delta V + \delta W_{nc} \tag{2.2}$$

where V is the potential of the applied conservative forces and δW_{nc} is the virtual work of the nonconservative forces during virtual displacements. Substituting Eqn. (2.2) into Eqn.(2.1),one obtains

$$\delta \int_{t_0}^{t_f} (\prod - T)dt - \int_{t_0}^{t_f} \delta W_{nc} dt = 0 \tag{2.3}$$

where $\prod$ is the total potential energy of the system .Above equation reduces to the static case when the kinetic energy vanishes and the remaining terms are invariant with time.

Here viscous damping forces will be the only nonconservative forces considered. Introducing the discretization into the kinetic energy and the virtual work of nonconservative forces:

$$\prod = \prod(\bar{u}) = \sum_{e=1}^{m} \prod^{e}(\bar{u}^{(e)}) \tag{2.4}$$

$$T = T(\dot{\bar{u}}) = \sum_{e=1}^{m} T(\dot{\bar{u}}^{(e)}) = \frac{1}{2}\int_{v} \rho \dot{u}^{T} \dot{u} dV$$

$$= \sum_{e=1}^{m} \frac{1}{2} \dot{\bar{u}}^{(e)T} M^{(e)} \dot{\bar{u}}^{(e)} \tag{2.5}$$

$$\delta W_{nc} = \sum_{e=1}^{m} \int_V \delta u^T (-c_s^{(e)} \dot{u}) dV$$

$$= -\sum_{e=1}^{m} \delta \bar{u}^{(e)} C^{(e)} \dot{\bar{u}}^{(e)} = -\sum \delta \bar{u}^{(e)} f_d^{(e)} \qquad (2.6)$$

where $\bar{u}$ and $\dot{\bar{u}}$ are the nodal displacement and velocity vectors, respectively, and $M^{(e)}$ and $C^{(e)}$ are respectively the consistent mass and damping matrices for element e ,given by:

$$M^{(e)} = \int_V \rho^{(e)} N^T N dV \qquad (2.7)$$

$$C^{(e)} = \int_V c_s^{(e)} N^T N dV \qquad (2.8)$$

where $\rho^{(e)}$ and $c_s^{(e)}$ are the mass density and the viscous damping coefficient for element e, and N is the matrix of shape functions. The minus sign is used in Eqn (2.6) since the damping force(viscous damping which is proportional to the velocity is assumed) opposes the motion. Using Eqns.(2.4) through (2.6) in the variational principle (2.3),we obtain:

$$\int_{t_0}^{t_f} [\delta \bar{u}^T \frac{\partial U}{\partial \bar{u}} - \frac{\partial T}{\partial \bar{u}} + f_d - p] - \delta \dot{\bar{u}}^T \frac{\partial T}{\partial \dot{\bar{u}}}] dt = 0 \qquad (2.9)$$

where p is the vector of applied loads and f_d is the damping force vector (assembly of $f_d^{(e)}$ of Eqn. 2.6) associated with the generalized coordinates $\bar{u}$. Integrating the second term (involving

$\overline{u}$) of Eqn.(2.9) by parts and observing that $\delta\overline{u}$ vanishes at t = t_0 and t = t_f and arbitrary in the open interval (t_0,t_f), we obtain:

$$\frac{d}{dt}\left(\frac{\partial T}{\partial \dot{\overline{u}}}\right)+\frac{\partial U}{\partial \overline{u}}-\frac{\partial T}{\partial \overline{u}}=p-f_d \tag{2.10}$$

which is a statement of Lagrange's equations. From this we can derive the governing differential equations of motion(the dynamic equilibrium equations)

$$\mathbf{M}\,\ddot{\mathbf{u}} + \mathbf{C}\dot{\mathbf{u}} + \mathbf{K}\,\mathbf{u} = \mathbf{p(t)} \tag{2.11}$$

where **M**, **C** and **K** are respectively the global mass, damping and stiffness matrices(made up by a proper assembly of the element matrices), **p(t)** is the time-dependent applied force vector, and $\ddot{\mathbf{u}}$, $\dot{\mathbf{u}}$ and **u** are the nodal acceleration, nodal velocity and nodal displacement vectors, respectively(the bar is dropped for convenience, i.e., u≡$\overline{u}$).

2.2.2 DIRECT TRANSIENT ANALYSIS

As shown, the governing differential equation of motion can be written as:

$$\mathbf{M}\ddot{\mathbf{u}} + \mathbf{C}\dot{\mathbf{u}} + \mathbf{K}\mathbf{u} = \mathbf{p(t)}$$

The corresponding initial conditions can be written as:

$$u(o) = d_o$$

and

$$\dot{u}(o) = v_o$$

where d_o and v_o are the given initial displacement and velocity vectors, respectively. Direct transient analysis is based on direct integration of the equation of motion, i.e. no prior transformation or eigenvalue analysis is required.

In NISA, Newmark method is used for direct transient analysis, which can be summarized by the following equations:

$$M\ddot{u}_n + C\dot{u}_n + Ku_n = p_n \tag{2.12}$$

$$u_{n+1} = u_n + \Delta t\, \dot{u}_n + (\tfrac{1}{2} - \beta)\Delta t^2\, \ddot{u}_n + \beta \Delta t^2\, \ddot{u}_{n+1} \tag{2.13}$$

$$\dot{u}_{n+1} = \dot{u}_n + (1-\gamma)\Delta t\, \ddot{u}_n + \gamma \Delta t \ddot{u}_{n+1} \tag{2.14}$$

where u_n,$\dot{u}_n$ and $\ddot{u}_n$ are the known solutions for u, $\dot{u}$ and $\ddot{u}$ at time step n, respectively. The parameters β and γ determine the stability and accuracy characteristic of the algorithm. In NISA, the Newmark method is implemented with displacement form. The predictor are defined as:

$$\hat{\dot{u}}_{n+1} = \dot{u}_n + (1 - \gamma)\Delta t\, \ddot{u}_n$$

$$\hat{u}_{n+1} = u_n + \Delta t\, \dot{u}_n + (\tfrac{1}{2} - \beta)\Delta t^2\, \ddot{u}_n$$

With this and Eqns. (2.13) and (2.14) the velocity and the acceleration of the current time step can be written as:

$$\ddot{u}_{n+1} = \frac{1}{\beta \Delta t^2}\hat{u}_{n+1} - \frac{1}{\beta \Delta t^2}\hat{u}_{n+1} \tag{2.15}$$

$$\dot{u}_{n+1} = \hat{\dot{u}}_{n+1} - \frac{\gamma}{\beta \Delta t}\hat{u}_{n+1} + \frac{\gamma}{\beta \Delta t}\hat{u}_{n+1} \tag{2.16}$$

Substituting these into Eqn. (2.12),we have the following recursive equation to solve for displacement u_{n+1}:

$$(\frac{1}{\beta \Delta t^2}M + \frac{\gamma}{\beta \Delta t}C + K)u_{n+1} = p_{n+1} + (\frac{1}{\beta \Delta t^2}M + \frac{\gamma}{\beta \Delta t}C)\hat{u}_{n+1} - C\hat{\dot{u}}_{n+1} \tag{2.17}$$

By defining the effective stiffness matrix,

$$K^* = \frac{1}{\beta \Delta t^2}M + \frac{\gamma}{\beta \Delta t}C + K$$

and the effective load vector,

$$p^* = p_{n+1} + (\frac{1}{\beta \Delta t^2}M + \frac{\gamma}{\beta \Delta t}C)\hat{u}_{n+1} - C\hat{\dot{u}}_{n+1}$$

then, Eqn. (2.17) becomes

$$K^{*}u_{n+1} = p^{*} \tag{2.18}$$

which is in the form of the familiar matrix equation for static analysis that can be solved for the displacement vector u_{n+1}. Eqns. (2.15) and (2.16) can then be used to solve for acceleration and velocity.

2.2.3 BODY FORCE

In NISA gravity loads and inertia loads(due to angular velocity and linear angular acceleration) may be applied to any element which possess a non zero mass density. With reference to Fig. 2.2, the XYZ system is the rotating frame of reference which rotates with an angular velocity ω and angular acceleration α about the X′Y′Z′ system. At the instant shown, the two systems are parallel to each other. A linear acceleration field a_L is also applied to the two systems.
The absolute acceleration of a generic point p can be written as:

$$a_p = a_L + \ddot{u} + \wedge r + \Omega\Omega r + 2\Omega\dot{u}$$

where

$$r = r_{po} - r_{o'o}$$

and

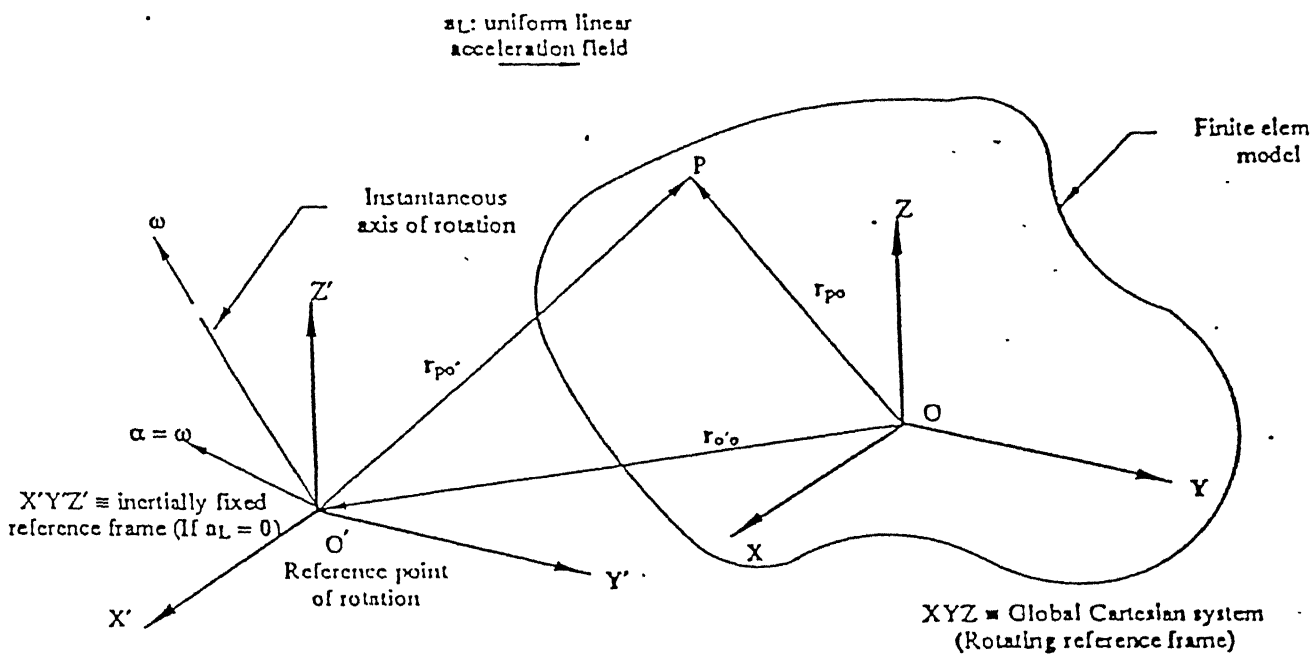

Fig. 2.2 Acceleration at a point due to linear and angular motion

$$\Omega = \begin{bmatrix} 0 & -\omega_z & \omega_y \\ \omega_z & 0 & -\omega_x \\ -\omega_y & \omega_x & 0 \end{bmatrix}.$$

$$\Lambda = \begin{bmatrix} 0 & -\alpha_z & \alpha_y \\ \alpha_z & 0 & -\alpha_x \\ -\alpha_y & \alpha_x & 0 \end{bmatrix}$$

a_L = the absolute acceleration of the moving frame of reference X′Y′Z′ due to the linear acceleration field.

$\ddot{u}$ = the stretching-term acceleration (i.e., relative) as viewed by an observer attached to the X′Y′Z′ system.

Λr = the tangential acceleration due to the angular acceleration α. For steady motion about a fixed axis, this term goes to zero.

$\Omega\Omega r$ = the centripetal acceleration (due to the angular velocity of the moving axes.)

$2\Omega\dot{u}$ = the Corriolis acceleration(due to the interaction between the angular velocity and the stretching velocity).

For linear static analysis, the terms involving $\dot{u}$ and $\ddot{u}$ are not considered, and the generic point is considered on the undeformed configuration.

2.2.4 NISA ELEMENTS

Following is the brief description of the NISA elements used for modeling:

2.2.4.1 3-D Beam Element (NKTP = 12)

This element (Fig. 2.3) is a 2-node prismatic 3-D beam element. The formulation includes stretching, bending and torsion effects. The transverse shear deformation effect is included as an option, The beam vertices may be offset from the corresponding nodal points and the centroid may be offset from the shear center. The element has end release capability. The deformation is characterized by three translations (UX, UY, UZ) and three rotations (ROTX, ROTY, ROTZ). The local x-axis of the beam is along the centroidal axis. The local y and z axes are user defined and are not necessary principal axes of the cross section.

2.2.4.2 3-D SPAR ELEMENT(NKTP = 14)

This element (Fig. 2.4) is a 2-node uniaxial tension-compression 3-D line element and is used to model space trusses. The element may be oriented any where in space. The element has three translational degrees of freedom per node (UX, UY, UZ).

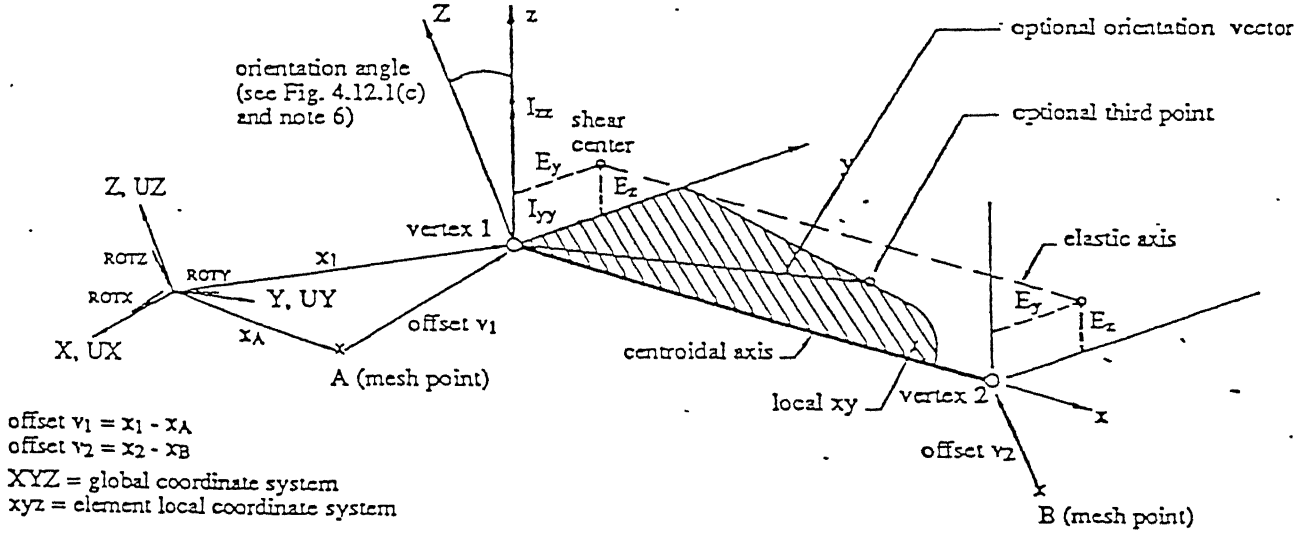

Fig. 2.3 Element configuration and orientation for 3D beam element, NKTP=12

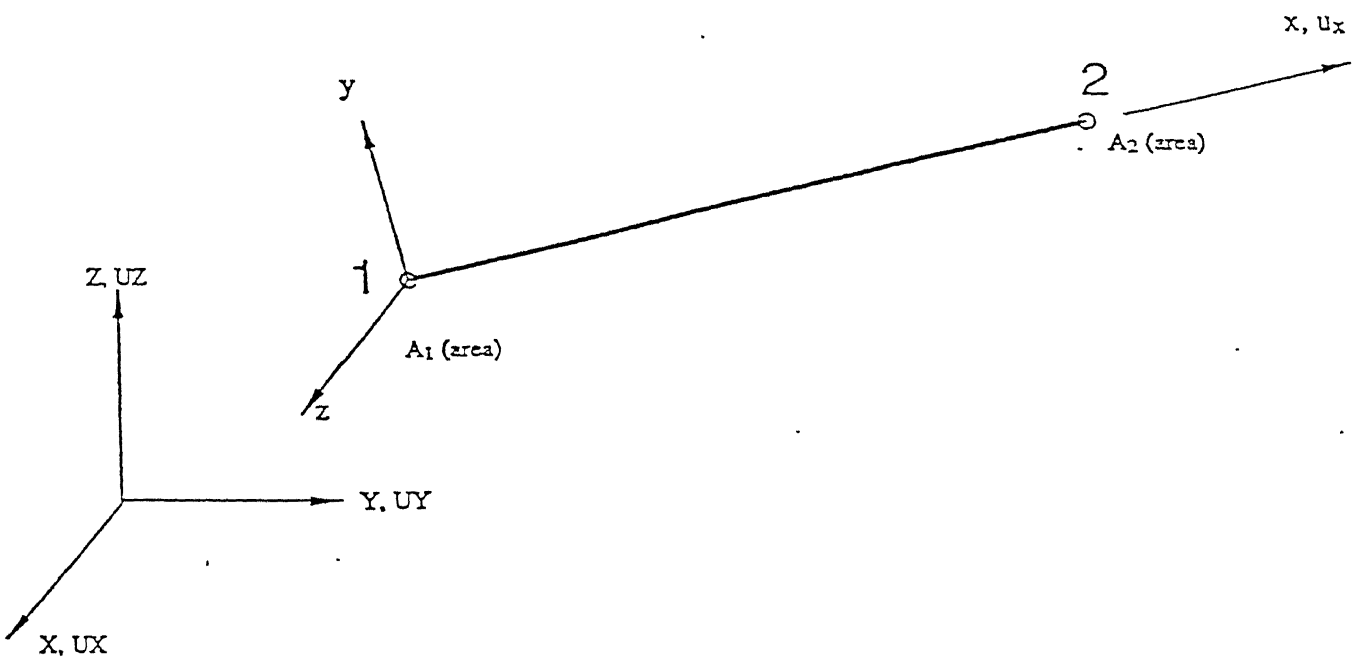

Fig. 2.4 Element configuration for 3D spar element, NKTP=14

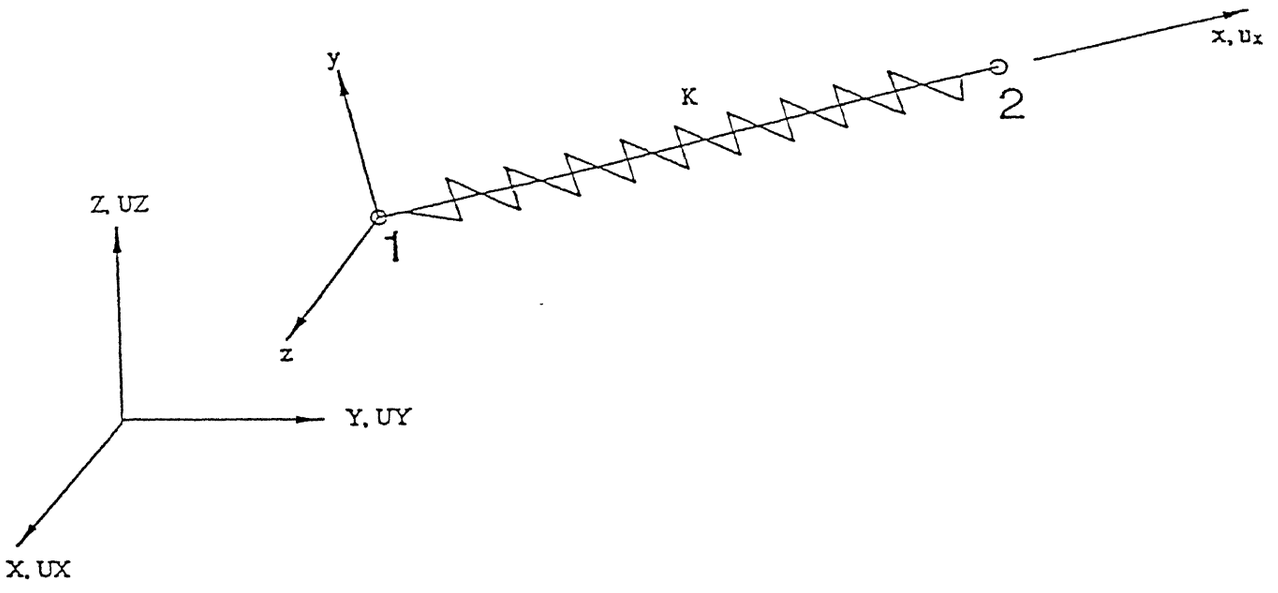

Fig. 2.5 Element configuration for 3D translational spring element, NKTP=17

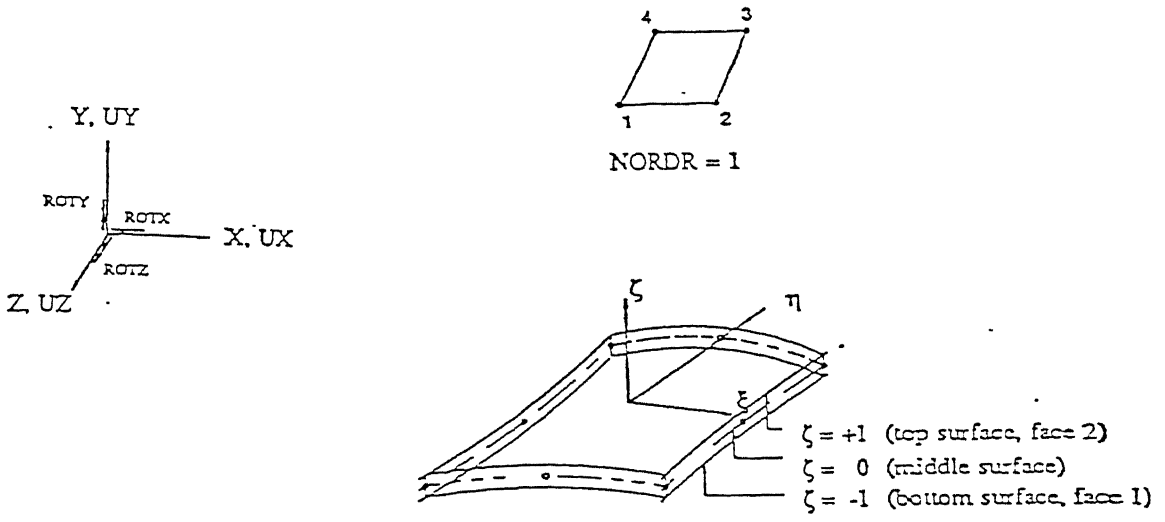

Fig. 2.6 Element configuration and face numbering convention for top and bottom surfaces of shell element, NKTP=20, NORDR=1

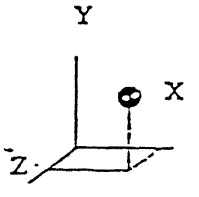

Fig. 2.7 Element configuration for 3D concentrated mass element, NKTP=26

2.2.4.3 3-D TRANSLATIONAL SPRING ELEMENT(NKTP = 17)

This element (Fig. 2.5) is a 2-node uniaxial tension-compression mass less spring in three dimension. The element may be oriented anywhere in space. The element has three translational degrees of freedom per node(UX, UY, UZ). The two nodes defining the spring may be coincident, in which case a direction vector is specified indicating the direction of the spring axis.

2.2.4.4 3-D SHELL ELEMENT(NKTP = 20)

The 3-D shell element (Fig. 2.6) includes membrane, bending and transverse shear deformation effects and is suited for modeling moderately thick to thin shell structures. The element has six degrees of freedom per node (UX, UY, UZ, ROTX, ROTY, ROTZ), but it posses no rotational stiffness about the normal to the shell surface.

The element can be shaped as a 4 to 12 node quadrilateral, or a 3 or 6 node triangle.

2.2.4.5 3-D CONCENTRATED MASS ELEMENTS(NKTP = 26)

The 3-D concentrated mass element (Fig. 2.7) provides a mean to represent the inertia properties of the model and to apply external loads due to body forces(e.g. gravity). The inertia properties

may also be represented by the mass density of the structural elements. This element has three degrees of freedom(UX, UY, UZ).

2.2.5 INPUT DATA SETUP FOR LINEAR DIRECT TRANSIENT DYNAMIC ANALYSIS

Fig. 2.8 shows a global description for the input data setup for a typical linear direct transient dynamic analysis run. The first data block (executive commands) must flag the analysis type as linear direct transient and should include appropriate or applicable commands for file saving, element resequencing etc..

The second data block (the model data) should start with the *TITLE data group in order to allow printing of the problem as a heading on all pages of the output file. The model data then describes model characteristics, as for example: element definition (*ELEMENT), nodal coordinates (*NODES), material properties(*MATERIAL),etc.. Some kinematic constraints are considered to be model characteristics and properties in this block, namely: the rigid element data(*RIGLINK), the multi-point constraint equations(*MPCEQN) and the couple displacement data (*CPDISP). Other general groups such as definition of vectors and sets (*VECTORS and *SETS, respectively) are also defined in this block.

The third data block (the analysis data) should start with *EVENT data group. An event title is available on the *LCTITLE data group. The block then describes various loading, kinematic boundary conditions and initial conditions of the structure. The initial condition data (*INTIAL) can appear before the *EVENT data group or in the first event. Loading include, for example, concentrated force (*CFORCE) and body force(*TBODYFORCE). Kinematic boundary conditions only contain the specified displacement data (*SPDISP). The block defines various output and print control options. It should be noted that the specified displacement data, *SPDISP, cannot be changed from one event to another.

The last card of the input deck must always be the input data terminator, the *ENDDATA data group.

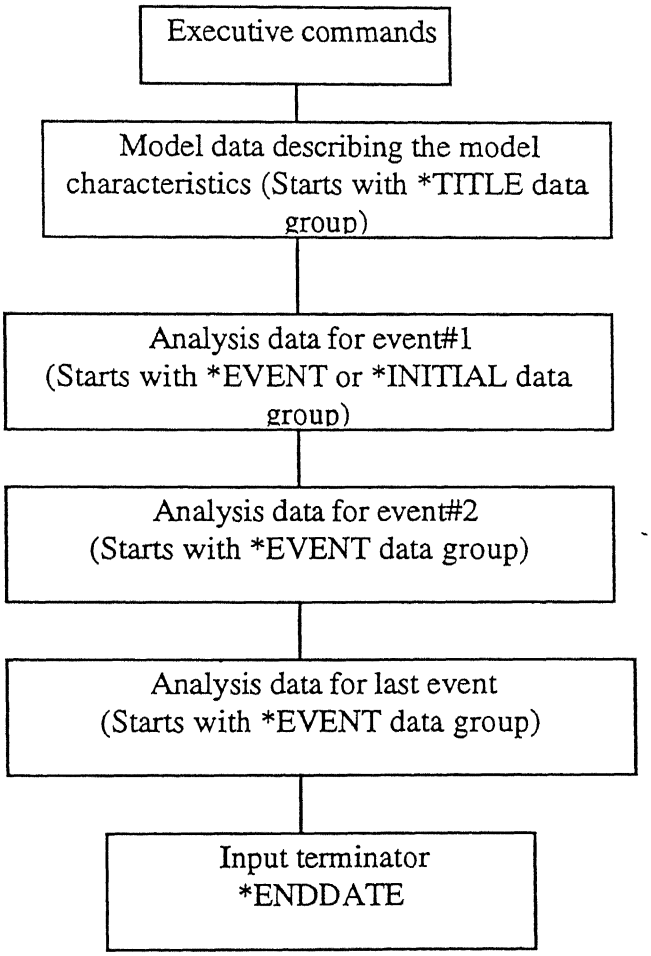

Fig. 2.8 Input data setup for linear transient dynamic analysis

CHAPTER - 3

MODELING OF CHASSIS FRAMES FOR NISA

3.1 INTRODUCTION TO THE CHASSIS FRAMES

Both the present chassis structures can be looked upon as a space frame consisting of 3-D beam elements, 3-D spar element, 3-D translational spring element, 3-D general shell element and 3-D concentrated mass element. Location of joints and directions of members are completely arbitrary, and the structure is designed to carry forces that are general in space.

3.1.1 SIDE MOUNTING MODEL

Fig. 3.1 shows the chassis of the three wheeler 'VIKRAM' (side mounting). It is made of a central tube through out the length of the vehicle. This tube can be called the central main element of the entire vehicle. Two channels running parallel to the tube are mounted to the tube through cross member, which is perpendicular to the tube attached to the tube. These cross members are also channel section having the same cross sectional area as that of side channel. A platform made of same cross section channel is supported by these side channels as well as two leaf springs in the rear part of the chassis(one on the each side). Other end of the leaf spring is attached to the axle

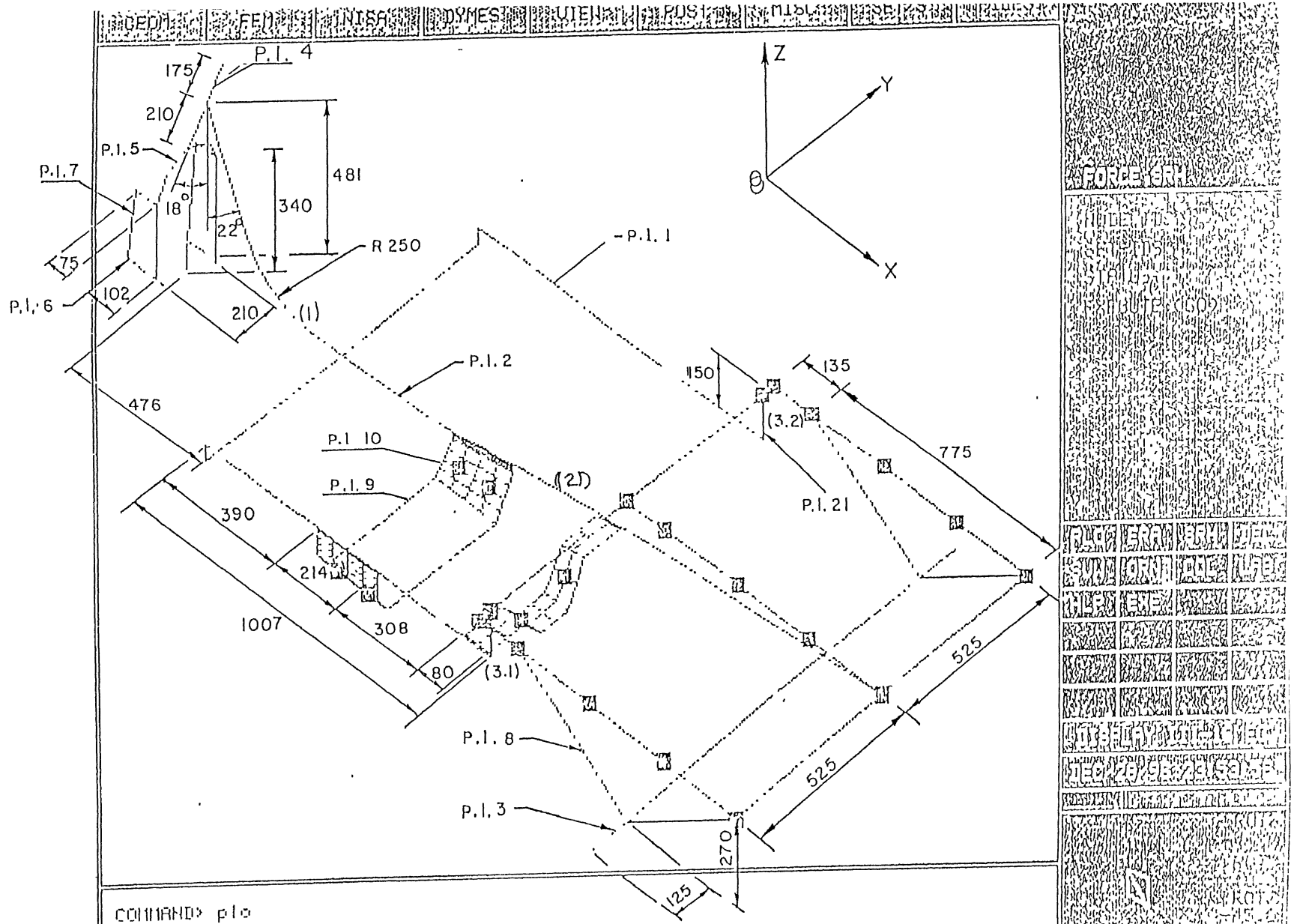

Fig. 3.1 Model for side mounting frame

P.I. → Property identification number

Number indicated in bracket → section number

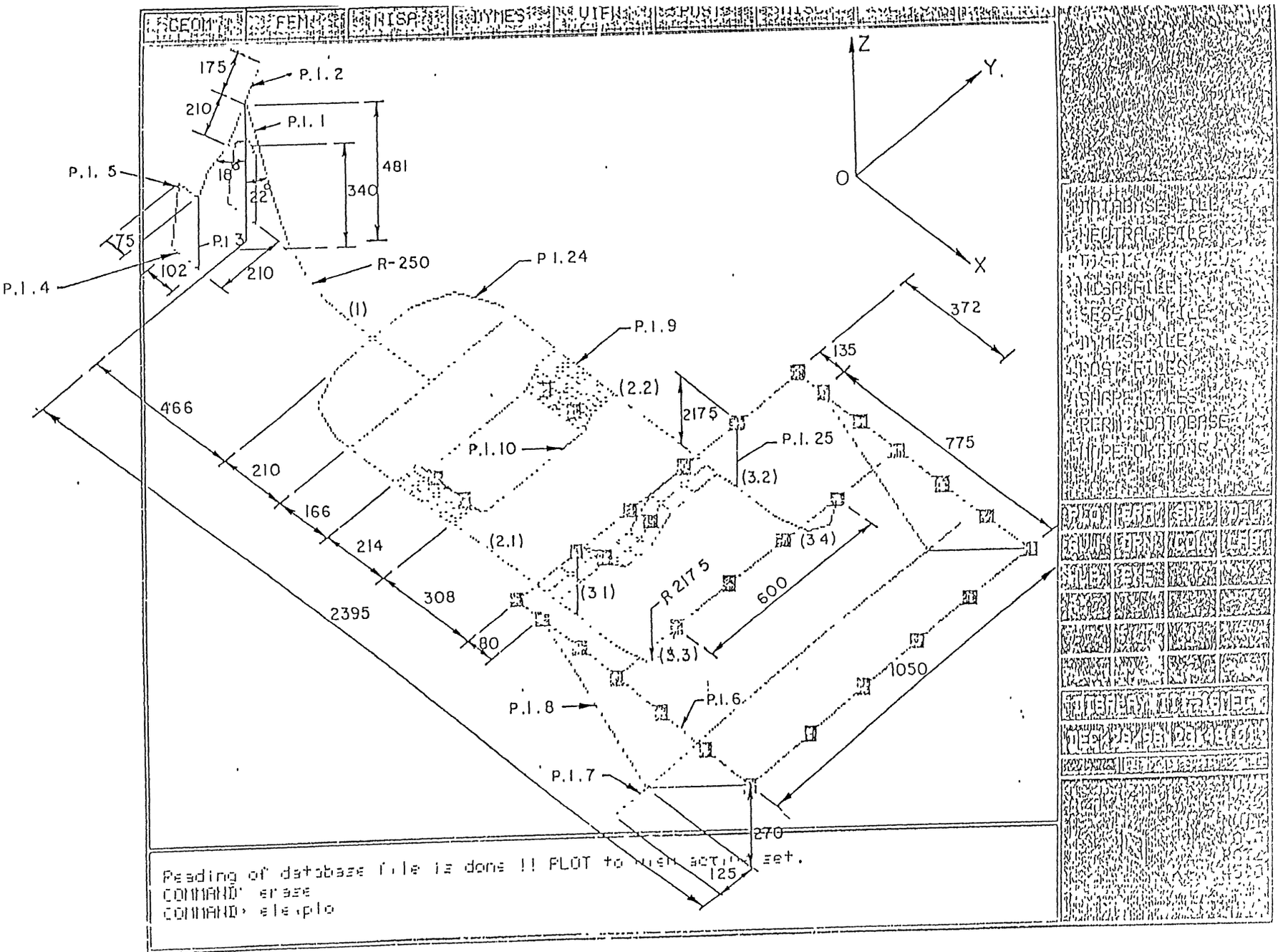

Fig. 3.2 Model for central mounting frame

P.I ⟶ Property identification number

Number indicated in bracket ⟶ section number

joining the two rear wheels. Engine and gear box is mounted between central tube and one of the side channels, on plate at six different supporting points. Front tire of the vehicle is attached to spring which is connected to a semicircular fork through spar elements. The middle point of this fork is attached to the central tube through another tube. Cross sectional properties for this model are given in the tables 3.1 to 3.5 and in the Fig. 3.10. Section 1, section 2, section 3.1 and section 3.2 (Fig. 3.1) are critical sections for this model.

3.1.2 CENTRAL MOUNTING MODEL

Fig. 3.2 shows the another model of the chassis of the three wheeler 'VIKRAM' (central mounting). Front part of it is made of the central tube and is similar to the side mounting model. Central tube is cut when it becomes horizontal. It is joined to two tubes running parallel to each other in the horizontal plain, through cross members at two different points. These cross members are also tubes of same diameter. Rear platform is supported on parallel tubes as well as on two leaf springs (one on each side). Other end of the leaf spring is attached to the axle; joining the two rear wheels. Engine and gear box is mounted between two parallel tubes, on plates at six different supporting points. Cross sectional properties for this model are given in the tables 3.6 to 3.10 and in the Fig. 3.11. Section 1, section 2.1, section 2.2 and section 3.1 to section 3.4 (Fig. 3.2) are critical sections for this model.

3.2 ENGINE SPECIFICATIONS

Following are some particulars of the VIKRAM engine

Make: Greaves India Limited, Aurangabad

Type: Single cylinder, 4-Stroke air cooled diesel engine

Cylinder Bore: 85 mm

Stroke Length: 90 mm

Cubic Capacity: 510 cm^3

Max. Output: 11 H.P. at 3000 rpm

Max. Torque: 3 kg-m at 2000 rpm

Engine weight with gear box assembaly: 102 Kg

Speed range of the engine: 850-3200 rpm

Engine Power Pack Dimensions:

Engine height: 562 mm

Engine length: 753.6 mm

Engine width: 232 mm at mounting points

3.3 OTHER MISCELLANEOUS SPECIFICATION

Gear Ratios:

Different gears ratios are given as bellow:

1st gear = 1: 5

2nd gear = 1: 2.93

3rd gear = 1: 1.84

4th gear = 1: 1.29

Reverse gear = 1: 5.34

Secondary transmission (differential unit)

Ratio = 1 : 4.1

Wheel dia = 488 mm

Material of the chassis structure:

Entire chassis structure is made of oil quenched and tempered carbon steel with carbon contents up to 0.2%(max.). Various properties of the material are as follows:

Tensile strength: 640 Mpa

Yield stress: 440 Mpa

Specific Weight: $7.85 * 10^{-6}$ Kg/mm^3

Poisson's ratio: 0.292

Modulus of rigidity: $0.79 * 10^6$ Kgf/cm^2

Young's modulus: $2.07 * 10^8$ Kg/mm s^2

3.4 ENGINE FORCES AND MOMENTS

At engine mount system following external forces are introduced due to the weight and moments associated with the engine.

i. Weight of the engine:

The engine mass including the mass of the gear box is 102 Kgs. As a result 17 Kgs load is introduced at the six engine mounting points. But the magnitude of this force is small as compared to the dynamic forces taken up by the chassis.

ii. Reciprocating inertia forces, F_{rec} , in the engine:

These forces are given [5] as,

$$F_{rec} = M_{rec}\omega^2 r\{\cos(\omega t) + \frac{\cos(2\omega t)}{n}\} \quad (3.1$$

where,

M_{rec} : reciprocating masses (mass of piston = mass of gudgeon pin + 1/3 mass of con. rod)

ω: angular velocity of the engine crank shaft

r: radius of crank

n: connecting rod length / crank radius

A_p: Area of piston

l_p: connecting rod length

r: crank radius

n: l_p/r (equal to 4 for diesel engine)

For Aluminum piston [5]

$$M_{piston} = 0.43\ (0.00415\ D^3_{cylinder})$$

$$= 1.095 \text{ Kg.}$$

$$M_{con,rod} = 250\ A_p$$

$$= 1.42 \text{ Kg}$$

$$M_{rec} = 1.095 + (1.42/3)$$

$$= 1.568 \text{ Kg}$$

This force in the present system acts vertically. In balanced engine, half of the magnitude of primary forces are balanced by placing the required counter weight on the crank shaft. But in doing this balancing, another force in horizontal direction is generated, given by,

$$F_{hori} = (1/2)\, M_{rec}\omega^2 r \sin(\omega t) \qquad (3.2$$

iii. Forces due to rotating masses, F_{rot} , of the engine:

It is assumed that the present engine is balanced to the extent that C.G. of the crank shaft and the crank lies along its axis. So now the rotating forces, will stem from the portion of the mass of the connecting rod, M_{rot} , which can be assumed placed at the big end, will be responsible for centrifugal forces.

$$M_{rot} = (2/3)M_{con\ rod}$$

$$=0.94\ Kg$$

leading to,

$$F_{rot} = M_{rot}\, \omega^2\, r \sin(\omega t) \qquad (3.3)$$

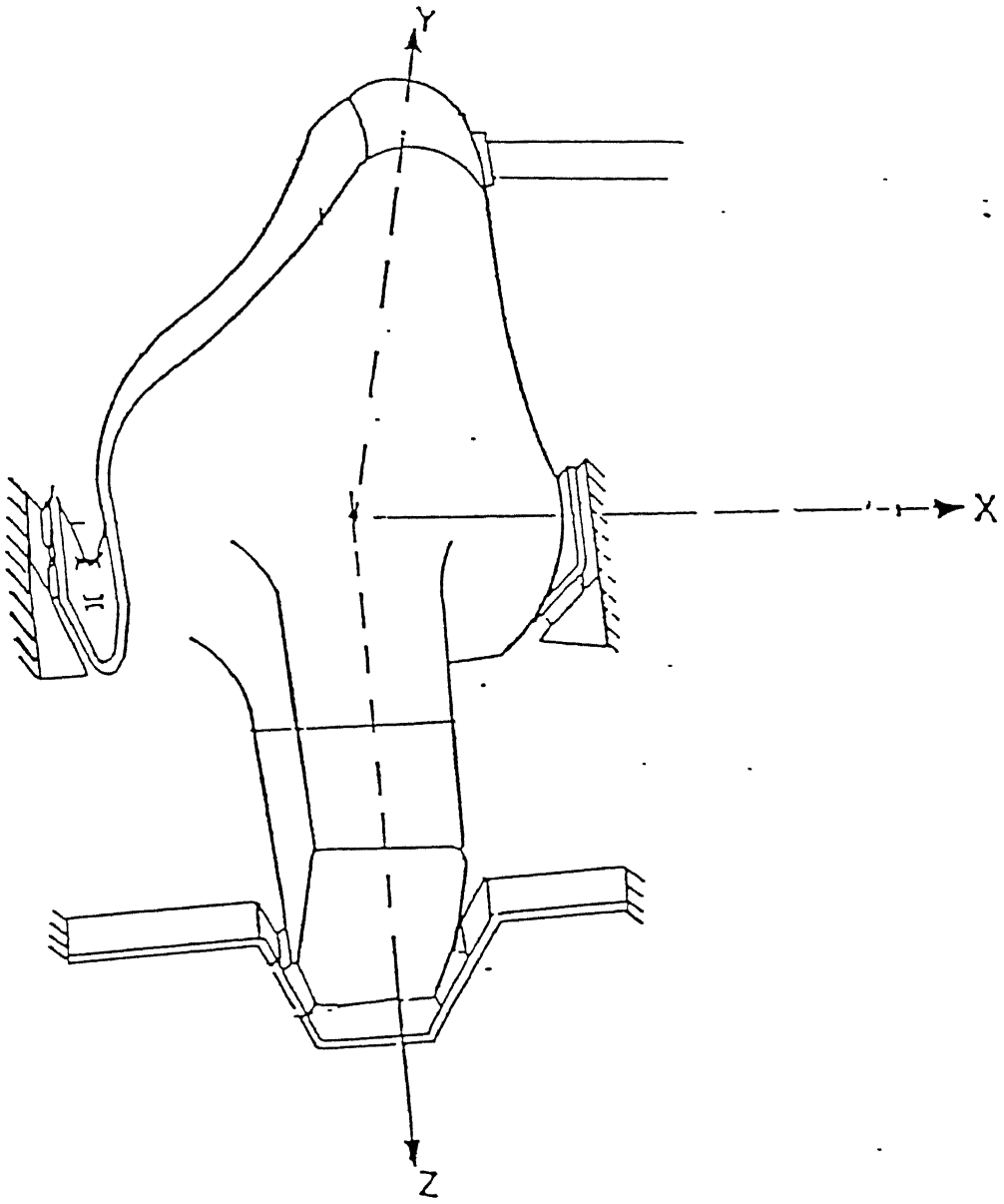

Fig. 3.3 Schematic diagram of Engine - mount

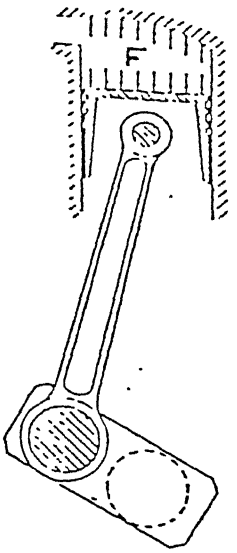

(a)

Piston-cylinder arrangement

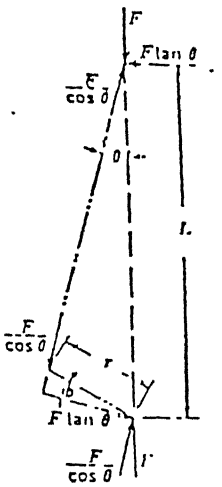

(b)

Forces coming on the engine

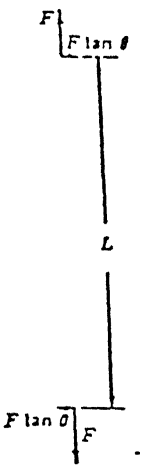

(c)

Forces coming on the engine-mount

Fig. 3.4 Forces resulting in the engine

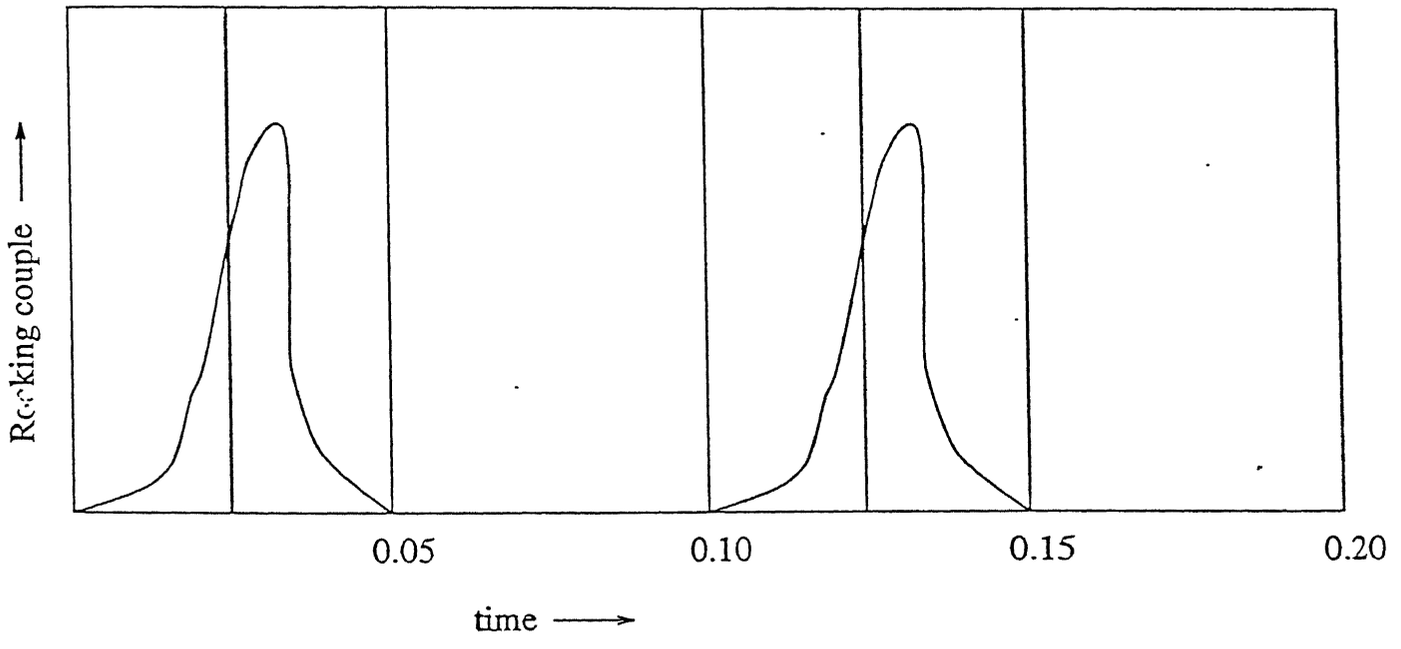

Fig. 3.5 Nature of rocking couple for 4-stroke engine at 1200 rpm

iv. Rocking Moment of the engine:

In the engine, at the end of compression stroke, due to explosion inside the cylinder, a lateral force normal to the cylinder axis acts on the piston, besides the thrust in the connecting rod. As a reaction to this lateral force , and opposing force acts on the cylinder walls. Figs. 3.4 b and 3.4 c shows the two forces F and F tanθ acting on the engine and the engine mounting supports respectively The force F acts upwardly on the cylinder head, is balanced by equal , down ward directed force on the crankshaft bearing. The summation of vertical forces for a engine structure is thus zero. The lateral force F tanθ, spaced L distance apart, results in a moment about crank shaft axis. As a result , whole of the engine rocks. The nature of this moment is shown in Fig.3.5. This rocking moment is assumed to be composed of a constant component and a harmonic component. The engine being a 4 stroke engine, the frequency of harmonic component is half the engine speed, as this moment is dependent on the explosion frequency i.e. firing frequency. The rocking moment is assumed to be maximum at 20^0 (assuming maximum pressure of about 60 bar inside the cylinder at around 20^0 [5]) crank angle as the explosion pressure is maximum around that crank angle.

Maximum explosive force generated inside the engine,

$$F_{max} = p_{max} A_p$$

$$= (60 * 10^5) 0.0056$$

$$= 34344 \text{ N}$$

Rocking moment,

$$M_z = (1/2)\, F_{max}\, l_{con} \tan(20^0)\, [\, 1 + \sin(\omega t/2)]$$

$$= (1/2)\ (34344)\ 0.18\ \tan(20^0)[\, 1 + \sin(\omega t/2)\,]$$

$$= 1124.5\, [\, 1 + \sin(\omega t/2)\,] \qquad (3.4$$

So the net vertical force,

$$F_y = (\frac{1}{2} M_{rec} + M_{rot})\omega^2 r \cos(\omega t)$$

$$= 1.724\ \omega^2 r \cos(\omega t) \qquad (3.5$$

and the net horizontal force,

$$F_x = (M_{rot} - \frac{1}{2} M_{rec})\omega^2 r \sin(\omega t)$$

$$= 0.16\ \omega^2\, r \sin(\omega t) \qquad (3.6)$$

3.5 LEAF SPRING MODELING

Two leaf springs support the rear platform of the chassis, one on each side. For the leaf springs the distance between two supporting points is 775 mm and the vertical distance of supporting point to the point which is attached to the axle is 270 mm.

While modeling for leaf spring it is assumed that both ends of the leaf spring are fixed to the platform. During modeling each leaf spring of stiffness K is replaced by two transitional springs o stiffness K' each as shown in the Fig. 3.6

From simple calculation we obtain the relation between K and K' as:

$$K' = (K/2)\sec^2\theta$$

$$\therefore \text{ if } K = 5.13 * 10^4 \text{ N/m}$$

$$\text{then } K' = (5.13 * 10^4/2)(1 + 775/(2*270))$$

$$= 6.25 * 10^4 \text{ N/m}$$

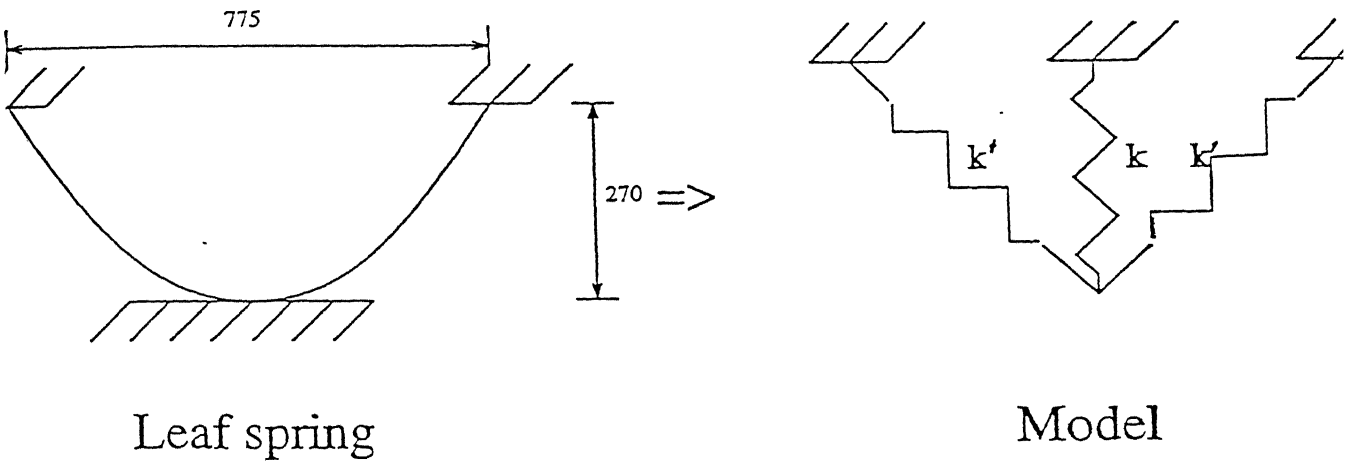

Fig. 3.6 Leaf spring modeling

3.6 BOUNDARY CONDITIONS

3.6.1 DISPLACEMENT BOUNDARY CONDITIONS

Since NISA does not provide the facility to model for tyre of an automobile the displacement boundary condition has been applied on the node at which tyres are mounted on the axle and the stiffness of the tube has not been considered. The following displacement boundary conditions have been applied for three different cases:

Idling:

CASE I

In case I a stationary vehicle with idling engine is simulated. For this all the six degrees of freedom of the rear tires' mounting node are assigned zero. Since front tire is mounted on spar element its all three translational degrees of freedom at that node are also zero.

Ditch:

While simulating a ditch it has been assumed that when the vehicle goes into the ditch it is running at the linear speed of 40 km./hr. in the fourth gear. A ditch has been simulated with a 2 m

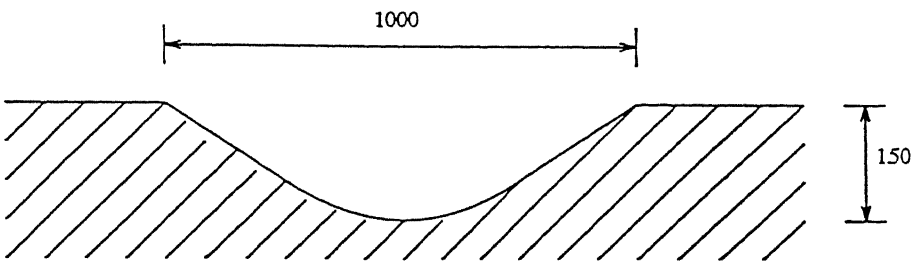

Fig. 3.7 Line diagram for the ditch

wavelength half sine wave of 15 cm amplitude. Wheel does not loose contact with the ditch surface while going through it.

Related calculations are:

Speed of the vehicle = V = 40 Kms/hr = 11.11 m/s

Time period = 2/11.11 = 0.18 sec

Time taken by wheel while traveling through ditch = 0.09 sec

Frequency = f = 1/T = 1/0.18

$\therefore \quad \omega = 2\pi f = 34.9$ rad/sec

$\therefore$ for motion through ditch

$$z = 150 \sin(\omega t)$$

CASE II

In case 2 a vehicle with front wheel passing over a ditch has been simulated. In this case front wheel's mounting node has been given displacement of

$$z = 150 \sin(\omega t)$$

where $\omega = 34.9$ rad./sec.

in the z direction. Other two degrees of freedoms for it are zero. All the six degrees of freedom of rear wheel's mounting node are also zero.

CASE III

In this case rear wheels' mounting nodes have been given displacement of

$$z = 150 \sin(\omega t)$$

where ω = 34.9 rad./sec.

in the z direction. All the other degrees of freedom for it are zero. All the three degrees of freedom for front wheel's mounting node are also zero.

3.6.2 FORCE BOUNDARY CONDITIONS

Static forces:

3-D point mass element has been used for specifying the static forces. Following types of static forces are acting on the frame for all the three cases:

Engine and gear box weight:

Total weight of the engine and gear box is 102 Kgs. which is equally distributed on six nodes (six supporting points) of the shell elements on which engine and gear box is resting.

Passenger load:

Passenger load of 700 Kgs. is assumed on the platform for doing the analysis. On each node of the platform certain load has been assigned proportional to the area supported by it (calculated after generating the proper mesh).

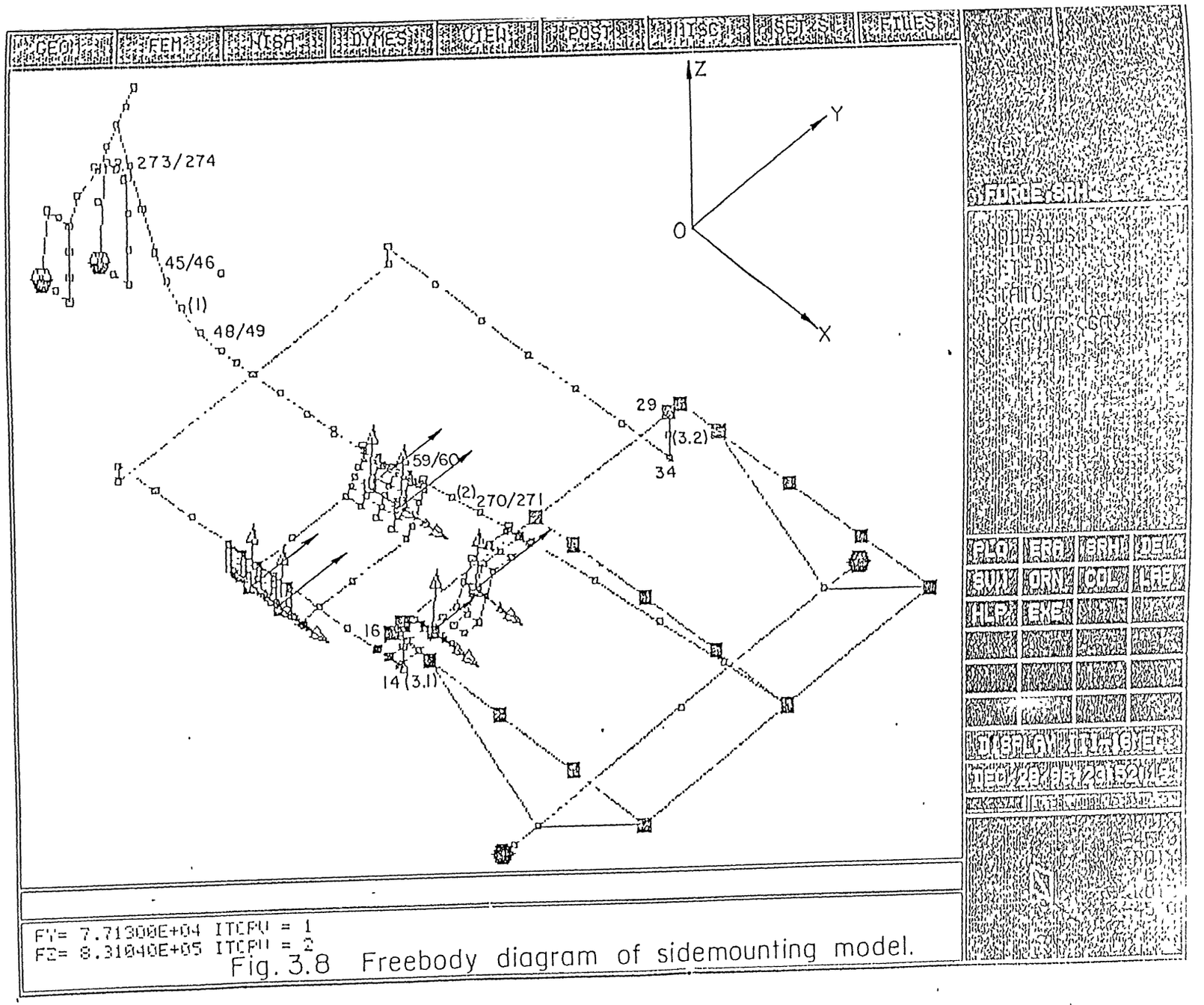

Fig. 3.8 Freebody diagram of sidemounting model.

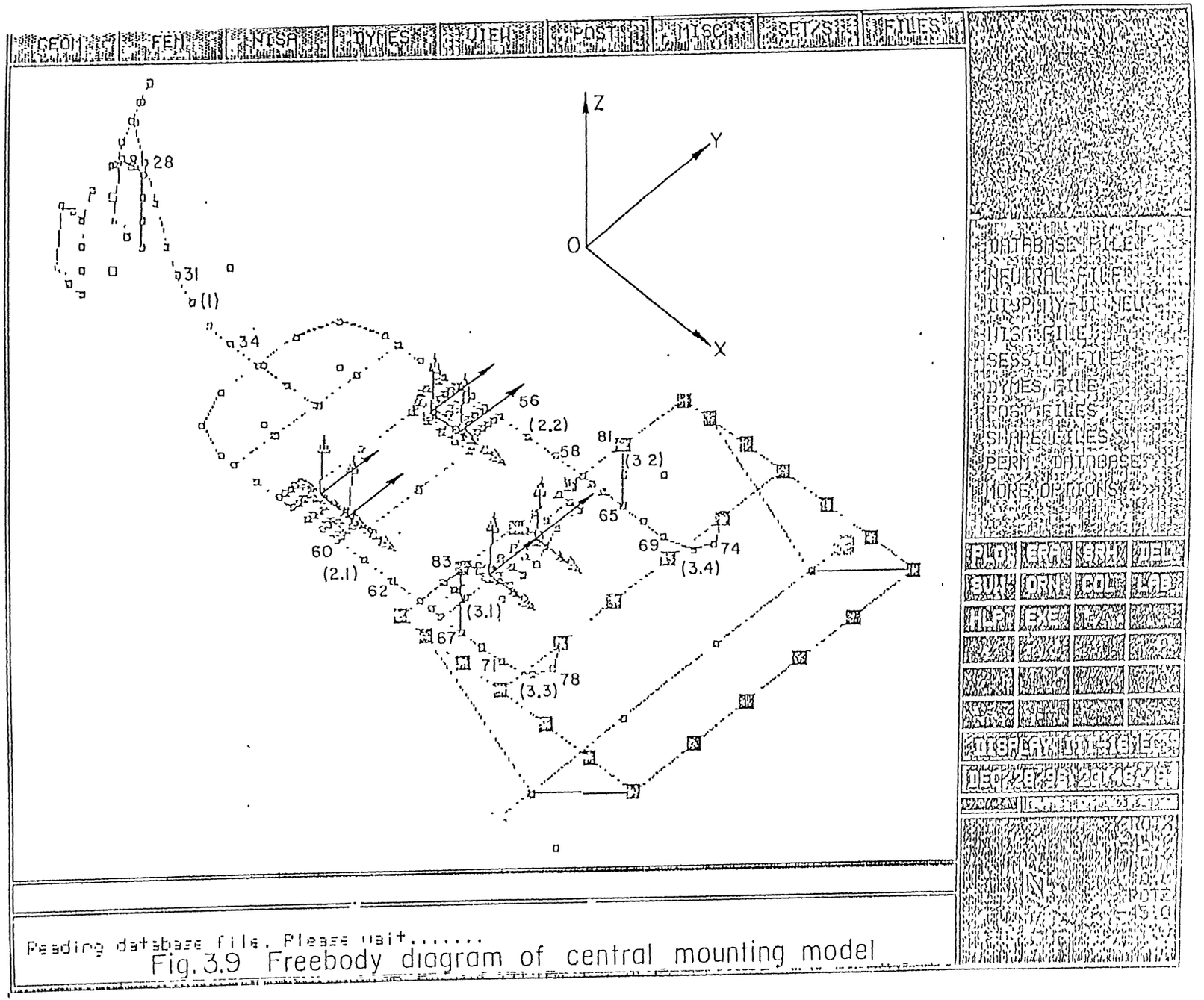

Fig. 3.9 Freebody diagram of central mounting model

Gravity force:

NISA provides facility to specify the body forces for the non-zero density structure. Gravity forces has been specified by using this facility for all the three cases.

Dynamic forces:

Engine unbalance forces:

Engine unbalance forces as described in the Eqns. (3.4), (3.5) and (3.6) are applied equally on six nodes of the shell elements on which engine and gear box is resting. Calculation of engine unbalance forces is done at following frequency:

Idling:

CASE I

Idling frequency of the engine is 14.25 Hz. All the unbalance forces for case I are calculated on this frequency.

Ditch:

CASE II

For this case engine speed for calculating the engine unbalance forces has been determined as follows:

Distance traveled by the rear wheel when the front wheel

passes over the ditch = v t

= 11.11*0.09

= 0.9999 m

Wheel periphery = π D

= π * 488

= 1533.1 mm

Number of revolution taken by rear wheel in 0.18 sec. = (2*999.9/1533.1)

= 1.305 rev.

∴ Wheel speed = 7.247 rev./sec.

∴ Engine speed = 7.247*4.1*1.29

= 38.3 Hz

∴ Unbalance forces for case II are calculated for engine speed of 38.3 Hz.

CASE III

In this case engine speed for calculating the engine unbalance forces has been determined as follows:

Length of the ditch curve = $\int ds$

$$= \int \sqrt{(dz)^2 + (dx)^2}$$

$$= \int \sqrt{(\frac{dz}{dt})^2 + (\frac{dx}{dt})^2}\, dt$$

$$= \int_0^{0.09} \sqrt{(150\omega \cos\omega t)^2 + v^2}\, dt$$

By applying trapezoidal rule for time step of 0.045 sec.

length of the ditch curve = 1053.29 mm

Wheel periphery = π D

= π * 488

= 1533.1 mm

Number of revolutions taken by rear wheel in 0.18 sec. = (2* 1053.29/1533.1)

= 1.37 rev.

$\therefore$ Wheel speed = 7.6288 rev./sec.

$\therefore$ Engine speed = 7.6288*4.1*1.29

= 40.35 Hz

$\therefore$ Unbalance forces for case II and case III are calculated for engine speed of 40.35 Hz.

3.7 DISCREATIZATION OF THE CHASSIS FRAME AND DATA INPUT TO NISA

For the finite element analysis the chassis is discretized into 254 elements and 280 nodes in the Side mounting model and into 236 elements and 241 nodes in the Central mounting model. The mass of the frame is applied through body force option of NISA. The various data input to NISA for the Side mounting frame is given in the tables 3.1 to 3.5 and for the Central mounting frame is given in the tables 3.6 to 3.10. Different input sections for modeling Side mounting frame are given in the Fig. 3.10 and for modeling Central mounting frame are given in the Fig. 3.11.

Prop. id.	A (mm^2)	I_{yy} (mm^4)	I_{zz} (mm^4)	I_{yz} (mm^4)	TSF (mm)	J (mm^4)	Pt. no.	SBFY	SBFZ
1	477	5.0e5	7.29e4	0.0	3	1431	1	0.0	0.0
							2	0.0	0.0
							3	0.0	0.0
							4	0.0	0.0
2	841	6.16e5	6.16e5	0.0	3.1e-5	1.23e6	1	0.0	4.7e-3
							2	4.7e-3	0.0
							3	0.0	4.7e-3
							4	4.7e-3	0.0
3	2827	1.27e6	1.27e6	0.0	-	6.27e5	1	0.0	2.3e-4
							2	2.3e-4	0.0
							3	0.0	2.3e-4
							4	2.3e-4	0.0
4	1963	6.13e5	6.13e5	0.0	-	3.82e6	1	0.0	3.3e-4
							2	3.3e-4	0.0
							3	0.0	3.3e-4
							4	3.3e-4	0.0
5	490	1.88e5	1.88e5	0.0	1.0e-4	3.82e4	1	0.0	4.0e-3
							2	4.0e-3	0.0
							3	0.0	4.0e-3
							4	4.0e-3	0.0
9	200	3.21e4	2.78e4	0.0	2	200	1	0.0	0.0
							2	0.0	0.0
							3	0.0	0.0
							4	0.0	0.0
21	504	4.5e5	2.16e5	0.0	6.7e-5	4.45e5	1	0.0	0.0
							2	0.0	0.0
							3	0.0	0.0
							4	0.0	0.0

Table no. 3.1 Input data for element with NKTP = 12 (Side mounting)

P.I.	A_1 (mm^2)	A_2 (mm^2)
6	125	125

Table no. 3.2 Input data for element with NKTP = 14 (Side mounting)

P.I.	K (kg/s^2)
7	7.66e3
8	6.25e4

Table no. 3.3 Input data for element with NKTP = 17 (Side mounting)

P.I.	Node no.	t (mm)
10	1	8
10	2	8
10	3	8
10	4	8

Table no. 3.4 Input data for element with NKTP = 20 (Side mounting)

P.I.	m (Kg.)
11	17
12	0.989
13	40.7
14	53.46
15	26.732
16	12.98
17	23.9835
18	69.877
19	91.787
20	45.89

Table no. 3.5 Input data for element with NKTP = 26 (Side mounting)

Prop. id.	A (mm^2)	I_{yy} (mm^4)	I_{zz} (mm^4)	I_{yz} (mm^4)	TSF (mm)	J (mm^4)	Pt. no.	SBFY	SBFZ
6	477	5.0e5	7.29e4	0.0	3	1431	1	0.0	0.0
							2	0.0	0.0
							3	0.0	0.0
							4	0.0	0.0
1	841	6.16e5	6.16e5	0.0	3.1e-5	1.23e6	1	0.0	4.7e-3
							2	4.7e-3	0.0
							3	0.0	4.7e-3
							4	4.7e-3	0.0
7	2827	1.27e6	1.27e6	0.0	-	6.27e5	1	0.0	2.3e-4
							2	2.3e-4	0.0
							3	0.0	2.3e-4
							4	2.3e-4	0.0
2	1963	6.13e5	6.13e5	0.0	-	3.82e6	1	0.0	3.3e-4
							2	3.3e-4	0.0
							3	0.0	3.3e-4
							4	3.3e-4	0.0
3	490	1.88e5	1.88e5	0.0	1.0e-4	3.82e4	1	0.0	4.0e-3
							2	4.0e-3	0.0
							3	0.0	4.0e-3
							4	4.0e-3	0.0
10	200	3.21e4	2.78e4	0.0	2	200	1	0.0	0.0
							2	0.0	0.0
							3	0.0	0.0
							4	0.0	0.0
25	504	4.5e5	2.16e5	0.0	6.7e-5	4.45e5	1	0.0	0.0
							2	0.0	0.0
							3	0.0	0.0
							4	0.0	0.0
24	575	2.68e5	2.68e5	0.0	5.7e-5	5.34e5	1	0.0	3.6e-3
							2	3.6e-3	0.0
							3	0.0	3.6e-3
							4	3.6e-3	0.0

Table no. 3.6 Input data for element with NKTP = 12 (Central mounting)

P.I.	A_1 (mm^2)	A_2 (mm^2)
4	125	125

Table no. 3.7 Input data for element with NKTP = 14 (Central mounting)

P.I.	K (kg/s^2)
5	7.66e3
8	6.25e4

Table no. 3.8 Input data for element with NKTP = 17 (Central mounting)

P.I.	Node no.	t (mm)
9	1	8
9	2	8
9	3	8
9	4	8

Table no. 3.9 Input data for element with NKTP = 20 (Central mounting)

P.I.	m (Kg.)
11	17
12	4.1
13	10.05
14	11.94
15	13.125
16	14.31
17	7.2
18	40.55
19	38.16
20	30.29
21	28.5
22	70.805
23	66.66

Table no. 3.10 Input data for element with NKTP = 26 (Central mounting)

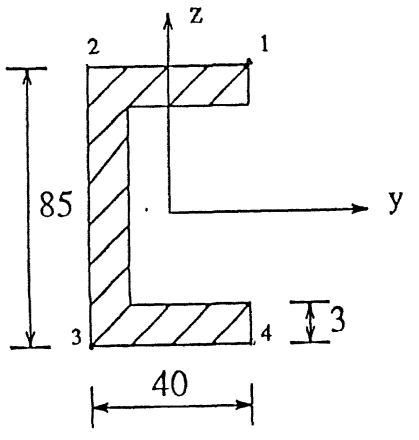

P.I. - 1

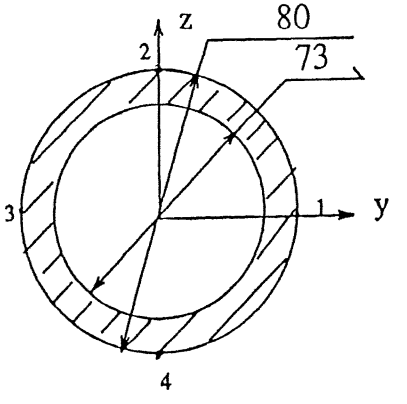

P.I. - 2

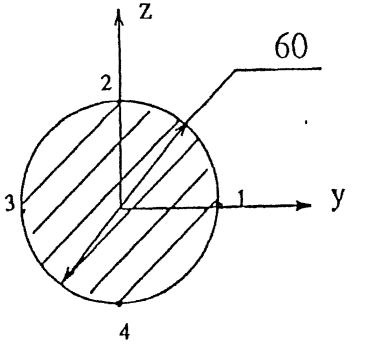

P.I. - 3

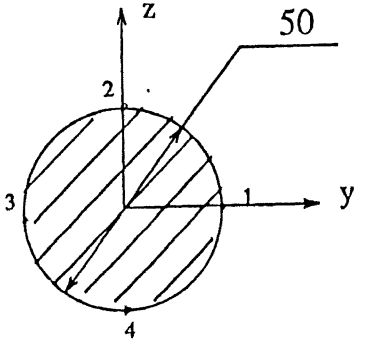

P.I. - 4

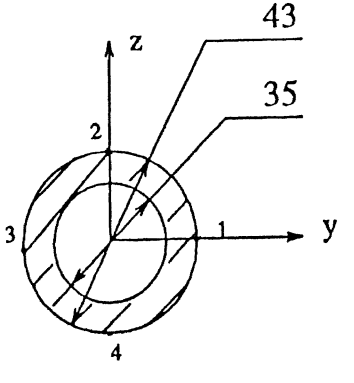

P.I - 5

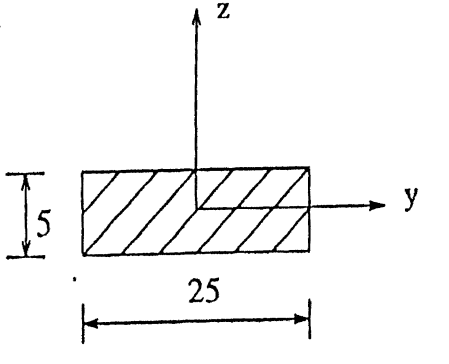

P.I. - 6

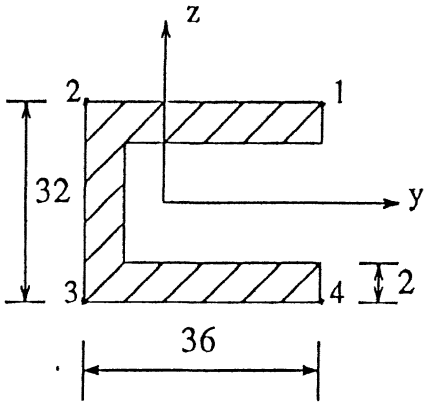

P.I. - 9

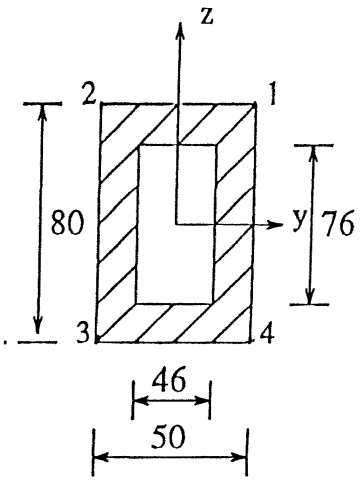

P.I. - 21

Fig. 3.10 Different input sections for sidemounting frame

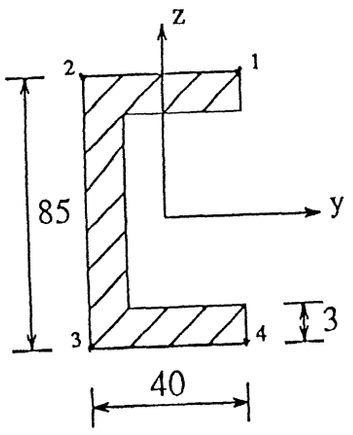

P.I. - 6

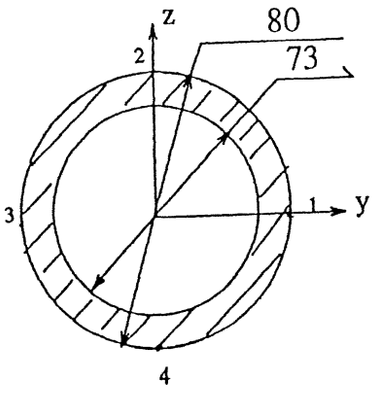

P.I. - 1

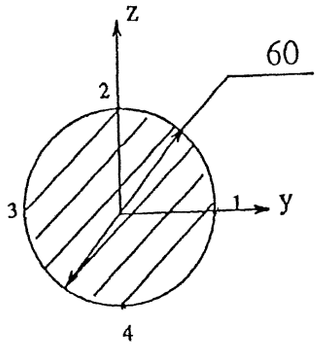

P.I. - 7

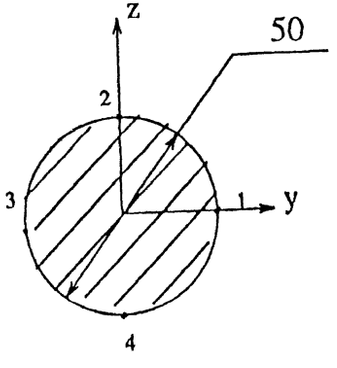

P.I. - 2

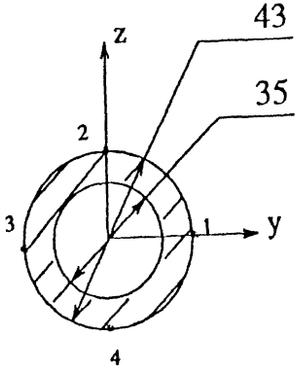

P.I. - 3

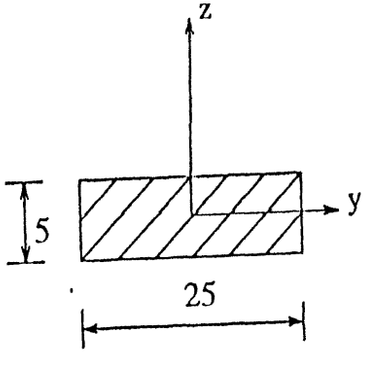

P.I. - 4

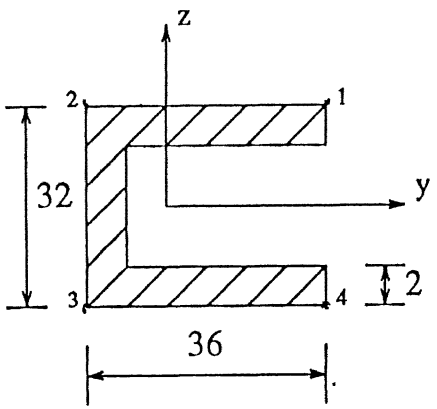

P.I. - 10

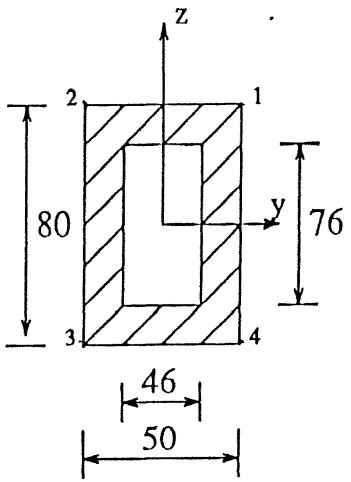

P.I. - 25

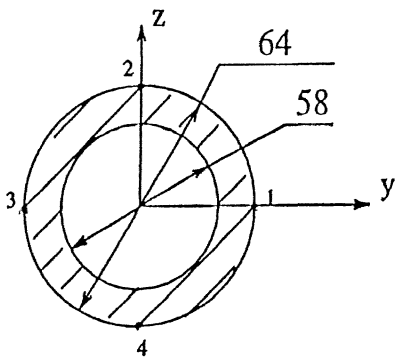

P.I. - 24

Fig. 3.11 Different input sections for centralmounting frame

CHAPTER - 4

THEORETICAL RESULTS

4.1 MAXIMUM SHEARING STRESS THEORY

Observations made in the course of extrusion tests on the flow of soft metals through orifices lend support to the assumption that the plastic state in such metal is created when the maximum shearing stress just reaches the value of the resistance of the metal against shear. Let σ_1 , σ_2 and σ_3 be the three principal stresses acting on three mutually perpendicular planes at a point in an isotropic material. Assuming $\sigma_1>\sigma_2>\sigma_3$, yielding , according to this theory occurs when the maximum shearing stress

$$\tau_{max} = \frac{\sigma_1 - \sigma_3}{2}$$

reaches a critical value. The maximum shearing stress theory is accepted to be fairly justified for ductile materials i.e. this theory says that if $\sigma_1>\sigma_2>\sigma_3$ are the three principal stress at a point, failure occurs when

$$\frac{\sigma_1 - \sigma_3}{2} \geq \frac{\sigma_y}{2}$$

where $\sigma_y/2$ is the shear stress at yield point in a uniaxial test.

4.2 RESULTS

NISA output gives us the maximum shearing stresses for maximum of four points on a given cross section. Since it is a 3-D combined bending and torsion problem so the maximum stress for a NISA beam element will occur on the surface of the element. By doing preliminary analysis four points on each cross section have been identified (Fig. 3.10 and Fig. 3.11) to represent that cross section for analysis for critical stresses. For Case I stress analysis has been done for one engine cycle and for Case II and Case III stress analysis has been done for the time for which vehicle passes over the ditch. In all the three cases total time span has been divided into eight steps for software to give the output. After sorting out the maximum shearing stresses on each cross section for selected nodes table has been formed for the sorted data. A computer program has been written to get the time Vs factor of safety data using maximum shearing stress theory. This data has been plotted using a software package.

Since it is a general 3-D structural dynamic force analysis it is expected that the maximum stress point at cross section will vary with time. This is verified by the data in the tables 4.1 to 4.6. At each cross section there is no fixed maximum stress point. Maximum stress point varies with time for a cross section. Also the time at which the maximum stress on a cross section for the whole duration of analysis occurs is different for different cross sections.

For Case I when the engine is idling and vehicle is stationary, maximum shearing stress for Side mounting frame occurs at node 273 for section 1, at node 59 for section 2, at node 14 for section

Node no. / Time (sec.)	273	45	48	59	270	14	16	34	29
1.755e-2	18e2 (3)	43e2 (4)	60e2 (4)	23e3 (1)	24e3 (1)	13e3 (1)	14e3 (1)	43e2 (2)	15e2 (3)
3.51e-2	44e2 (2)	46e2 (3)	59e2 (3)	57e3 (1)	57e3 (1)	22e3 (4)	18e3 (4)	15e3 (2)	58e2 (3)
5.265e-2	11e3 (3)	49e2 (3)	65e2 (2)	6e3 (1)	59e3 (1)	34e3 (4)	18e3 (4)	29e3 (2)	11e3 (3)
7.02e-2	15e3 (3)	49e2 (2)	40e2 (1)	32e3 (1)	31e3 (1)	41e3 (2)	13e3 (2)	34e3 (2)	12e3 (3)
8.775e-2	14e3 (3)	54e2 (3)	46e2 (4)	78e2 (4)	74e2 (2)	29e3 (2)	14e3 (2)	27e3 (3)	64e2 (3)
1.053e-1	98e2 (3)	51e2 (4)	70e2 (4)	12e3 (2)	12e3 (2)	48e2 (1)	72e2 (1)	96e2 (2)	30e2 (2)
1.228e-1	49e2 (3)	31e2 (3)	37e2 (3)	13e3 (3)	16e3 (3)	26e3 (2)	13e3 (2)	12e3 (3)	17e2 (3)
1.404e-1	49e2 (3)	53e2 (3)	81e2 (3)	36e3 (3)	4e3 (3)	34e3 (2)	3e4 (2)	22e3 (3)	41e2 (2)

Table no. 4.1 Variation of max. shearing stress (Kg/ s^2/mm) with time - Case I (Side mounting)

Node no. / Time (sec.)	28	31	34	60	62	56	58	67	83	65	81	71	78	69	74
1.755e-2	24e2 (3)	66e2 (4)	10e3 (2)	20e3 (4)	99e2 (4)	20e3 (4)	99e2 (4)	17e3 (2)	13e3 (2)	17e3 (3)	13e3 (3)	97e2 (2)	94e2 (4)	98e2 (2)	98e2 (2)
3.51e-2	13e2 (3)	12e2 (3)	14e2 (3)	39e3 (4)	18e3 (4)	37e3 (4)	17e3 (4)	42e3 (2)	43e3 (2)	41e3 (3)	44e3 (3)	37e3 (4)	37e3 (4)	42e3 (4)	47e3 (2)
5.265e-2	20e2 (2)	23e2 (4)	39e2 (4)	46e3 (2)	22e3 (2)	45e3 (2)	22e3 (2)	67e3 (1)	87e3 (2)	68e3 (4)	88e3 (3)	73e3 (1)	98e3 (4)	84e3 (3)	99e3 (2)
7.02e-2	25e2 (4)	50e2 (2)	90e2 (2)	33e3 (2)	18e3 (2)	37e3 (2)	19e3 (2)	85e3 (1)	10e4 (2)	86e3 (4)	10e4 (3)	88e3 (1)	11e4 (4)	10e4 (3)	11e4 (2)
8.775e-2	16e2 (3)	56e2 (2)	97e2 (4)	23e3 (2)	11e3 (2)	25e3 (2)	12e3 (2)	57e3 (1)	68e3 (2)	58e3 (4)	66e3 (3)	59e3 (1)	80e3 (4)	67e3 (3)	81e3 (2)
1.053e-1	33e2 (3)	11e2 (2)	44e1 (2)	51e2 (4)	21e2 (4)	30e2 (4)	13e2 (4)	30e2 (2)	15e2 (2)	49e2 (3)	33e2 (3)	14e2 (2	24e2 (4)	37e2 (1)	62e2 (4)
1.229e-1	57e2 (3)	59e2 (2)	94e2 (4)	13e3 (2)	73e2 (2)	12e3 (2)	72e2 (2)	46e3 (1)	49e3 (2)	44e3 (4)	49e3 (3)	45e3 (1)	61e3 (4)	47e3 (3)	55e3 (2)
1.404e-1	94e2 (3)	10e3 (4)	15e3 (4)	11e3 (1)	48e2 (1)	12e3 (3)	55e2 (3)	48e3 (1)	45e3 (2)	46e3 (2)	49e3 (1)	42e3 (1)	59e3 (4)	46e3 (3)	55e3 (2)

Table no. 4.2 Variation of max. shearing stress ($Kg/s^2/mm$) with time - Case I (Central mounting)

Node no. / Time (sec.))	274	46	49	60	271	14	16	34	29
1.125e-2	28e2 (1)	69e2 (4)	10e3 (4)	16e3 (3)	17e3 (3)	17e3 (2)	17e3 (2)	27e2 (2)	12e2 (3)
2.25e-2	10e2 (4)	10e2 (4)	23e2 (1)	43e3 (1)	42e3 (1)	16e3 (1)	15e3 (4)	65e2 (2)	34e2 (3)
3.375e-2	45e2 (3)	12e3 (4)	17e3 (4)	44e3 (1)	42e3 (1)	17e3 (2)	94e2 (2)	12e3 (2)	51e2 (3)
4.5e-2	45e2 (1)	20e2 (4)	30e2 (1)	23e3 (1)	23e3 (1)	22e3 (2)	18e3 (2)	16e3 (2)	77e2 (3)
5.625e-2	56e2 (4)	93e2 (4)	12e3 (1)	11e3 (3)	11e3 (3)	21e3 (4)	93e2 (1)	17e3 (3)	57e2 (3)
6.75e-2	56e2 (3)	79e2 (4)	12e3 (4)	16e3 (1)	16e3 (1)	15e3 (4)	71e2 (4)	20e3 (3)	36e2 (2)
7.875e-2	48e2 (3)	72e2 (3)	10e3 (3)	46e3 (1)	43e3 (1)	17e3 (2)	10e3 (2)	20e3 (2)	46e2 (3)
9e-2	84e2 (3)	75e2 (2)	11e3 (2)	40e3 (1)	38e3 (1)	14e3 (2)	15e3 (2)	19e3 (2)	59e2 (3)

Table no. 4.3 Variation of max. shearing stress ($Kg/s^2/mm$) with time - Case II (Side mounting)

Node no. / Time (sec.)	28	31	34	60	62	56	58	67	83	65	81	71	78	69	74
1.125e-2	33e2 (3)	99e2 (2)	15e3 (3)	25e3 (4)	12e3 (4)	13e3 (4)	75e2 (4)	19e3 (2)	73e2 (2)	12e3 (3)	13e3 (3)	82e2 (2)	36e2 (2)	52e2 (2)	44e2 (4)
2.25e-2	26e2 (3)	29e2 (3)	43e2 (2)	28e3 (4)	13e3 (4)	23e3 (4)	10e3 (4)	26e3 (2)	18e3 (2)	25e3 (3)	22e3 (3)	20e3 (4)	21e3 (4)	22e3 (3)	24e3 (2)
3.375e-2	36e2 (1)	71e2 (2)	10e3 (2)	22e3 (2)	99e2 (2)	33e3 (2)	14e3 (2)	34e3 (1)	46e3 (2)	36e3 (4)	41e3 (3)	36e3 (1)	50e3 (4)	45e3 (3)	52e3 (2)
4.5e-2	31e2 (3)	28e2 (2)	20e2 (3)	14e3 (2)	87e2 (2)	13e3 (3)	80e2 (2)	49e3 (1)	61e3 (2)	51e3 (4)	58e3 (3)	54e3 (1)	71e3 (4)	56e3 (3)	67e3 (2)
5.625e-2	35e2 (1)	40e2 (1)	41e2 (2)	16e3 (2)	10e3 (2)	15e3 (2)	99e2 (2)	50e3 (1)	60e3 (2)	47e3 (4)	61e3 (3)	51e3 (1)	67e3 (4)	55e3 (3)	66e3 (2)
6.75e-2	37e2 (3)	44e2 (2)	50e2 (2)	41e3 (4)	19e3 (4)	42e3 (4)	19e3 (4)	44e3 (2)	48e3 (2)	50e3 (3)	50e3 (3)	41e3 (3)	52e3 (4)	50e3 (1)	58e3 (2)
7.87e-2	30e2 (4)	90e2 (2)	13e3 (2)	42e3 (2)	18e3 (2)	42e2 (2)	18e3 (2)	36e3 (2)	43e3 (2)	38e3 (3)	42e3 (3)	34e3 (2)	48e3 (4)	44e3 (3)	51e3 (2)
9e-2	16e2 (3)	38e2 (2)	69e2 (2)	13e3 (2)	70e2 (2)	13e3 (2)	77e2 (2)	35e3 (1)	39e3 (2)	34e3 (4)	37e3 (3)	32e3 (4)	45e3 (4)	38e3 (3)	45e3 (2)

Table no. 4.4 Variation of max. shearing stress ($Kg/s^2/mm$) with time - Case II (Central mounting)

Node no. / Time (sec.)	274	46	49	60	271	14	16	34	29
1125e-2	29e2 (3)	71e2 (4)	10e3 (4)	16e3 (3)	18e3 (3)	18e3 (2)	17e3 (2)	29e2 (2)	11e2 (3)
225e-2	83e1 (3)	13e2 (3)	27e2 (3)	43e3 (1)	44e3 (1)	16e3 (4)	14e3 (4)	69e2 (3)	32e2 (3)
3375e-2	68e1 (2)	12e3 (2)	17e3 (4)	46e3 (1)	45e3 (1)	18e3 (2)	1e3 (2)	14e3 (2)	46e2 (3)
45e-2	12e3 (3)	52e2 (3)	2e2 (3)	27e3 (1)	27e3 (1)	26e3 (2)	1e3 (2)	19e3 (2)	72e2 (3)
56e-2	19e3 (3)	11e3 (4)	11e3 (4)	14e3 (1)	15e3 (1)	24e3 (4)	84e2 (1)	23e3 (3)	62e2 (3)
675e-2	27e3 (3)	14e3 (3)	11e3 (3)	28e3 (1)	26e3 (1)	23e3 (4)	1e4 (4)	29e3 (2)	59e2 (2)
7875e-2	35e3 (3)	19e3 (3)	15e3 (3)	43e3 (1)	39e3 (1)	28e3 (2)	15e3 (2)	3e3 (2)	75e2 (3)
9e-2	41e3 (3)	18e3 (3)	10e3 (3)	27e3 (1)	25e3 (1)	18e3 (2)	15e3 (2)	26e3 (2)	92e2 (3)

Table no. 4.5 Variation of max. shearing stress (Kg/s²/mm) with time - Case III (Side mounting)

Node no. / Time (sec.)	28	31	34	60	62	56	58	67	83	65	81	71	78	69	74
1.125e-2	33e2 (4)	10e3 (2)	15e3 (3)	26e3 (4)	12e3 (4)	13e3 (4)	74e2 (4)	18e3 (2)	83e2 (3)	12e3 (3)	12e3 (4)	78e2 (2)	36e2 (1)	58e2 (2)	52e2 (4)
2.25e-2	22e2 (1)	26e2 (2)	45e2 (2)	24e3 (4)	11e3 (4)	25e3 (4)	11e3 (4)	21e3 (2)	18e3 (2)	21e3 (3)	21e3 (3)	16e3 (4)	17e3 (4)	25e3 (1)	28e3 (2)
3.375e-2	22e2 (2)	70e2 (2)	11e3 (2)	20e3 (2)	90e2 (2)	32e3 (2)	13e3 (2)	30e3 (1)	44e3 (2)	40e3 (4)	40e3 (3)	30e3 (3)	43e3 (4)	46e3 (3)	56e3 (2)
4.5e-2	44e2 (3)	33e2 (4)	42e2 (1)	13e3 (1)	85e2 (2)	12e3 (2)	85e2 (2)	44e3 (1)	60e3 (2)	55e3 (4)	55e3 (3)	46e3 (1)	63e3 (4)	58e3 (3)	69e3 (2)
5.625e-2	94e2 (3)	34e2 (4)	24e2 (1)	16e3 (2)	10e3 (2)	21e3 (4)	12e3 (4)	46e3 (1)	60e3 (2)	59e3 (3)	60e3 (3)	45e3 (3)	60e3 (4)	58e3 (3)	69e3 (3)
6.75e-2	15e3 (3)	90e2 (3)	71e2 (4)	40e3 (2)	18e3 (2)	48e3 (4)	21e3 (4)	40e3 (2)	49e3 (2)	51e3 (3)	51e3 (3)	39e3 (4)	52e3 (4)	54e3 (1)	63e3 (2)
7.87e-2	22e3 (3)	11e3 (2)	15e3 (4)	35e3 (2)	15e3 (2)	41e3 (2)	17e3 (2)	35e3 (1)	45e3 (2)	45e3 (3)	45e3 (3)	35e3 (4)	51e3 (4)	48e3 (3)	57e3 (2)
9e-2	21e3 (3)	10e3 (3)	51e2 (4)	11e3 (1)	63e2 (2)	11e3 (3)	53e2 (2)	39e3 (1)	39e3 (2)	41e3 (4)	41e3 (3)	33e3 (2)	47e3 (4)	37e3 (3)	45e3 (2)

Table no. 4.6 Variation of max. shearing stress ($Kg/s^2/mm$) with time - Case III (Central mounting)

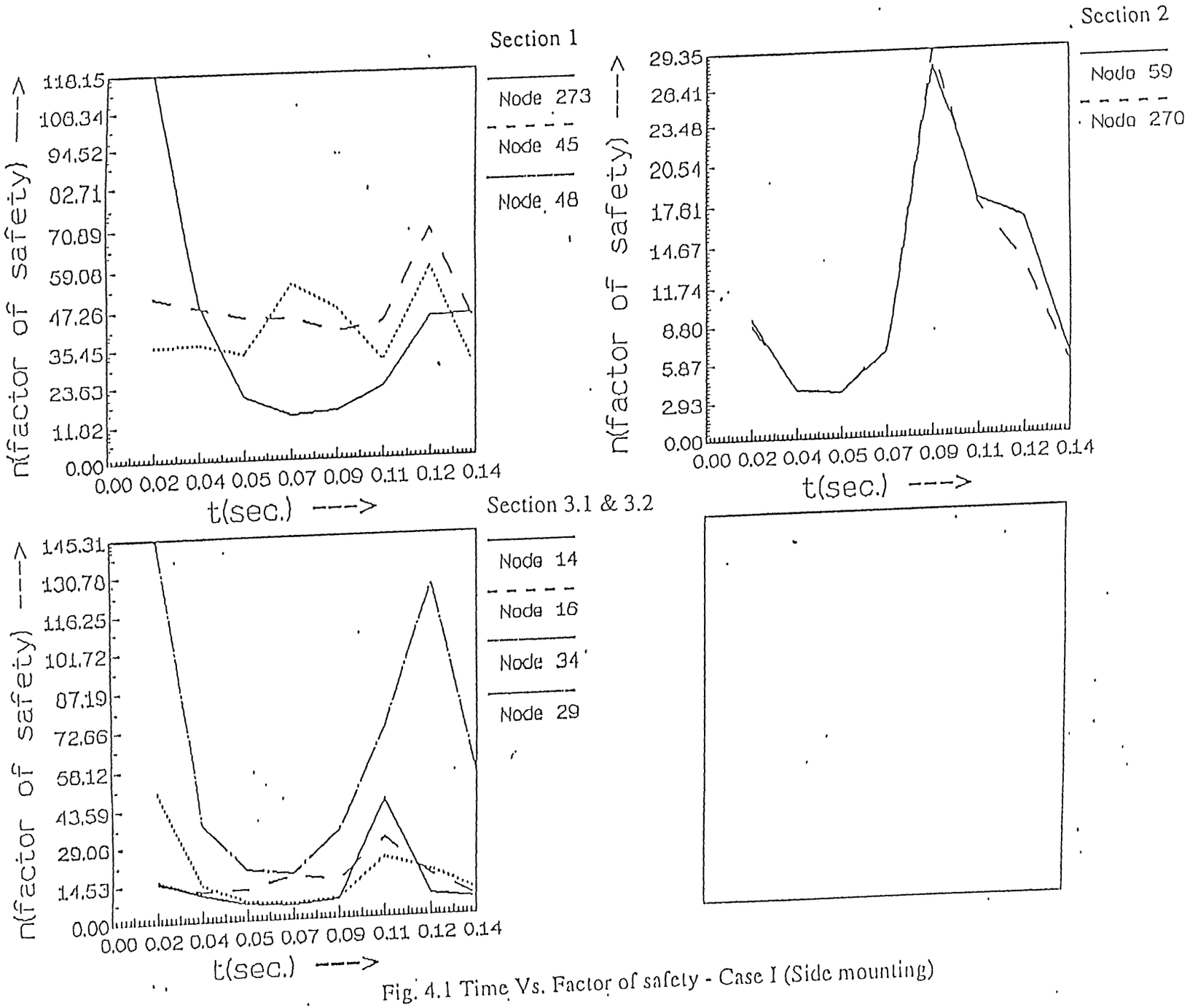

Fig. 4.1 Time Vs. Factor of safety - Case I (Side mounting)

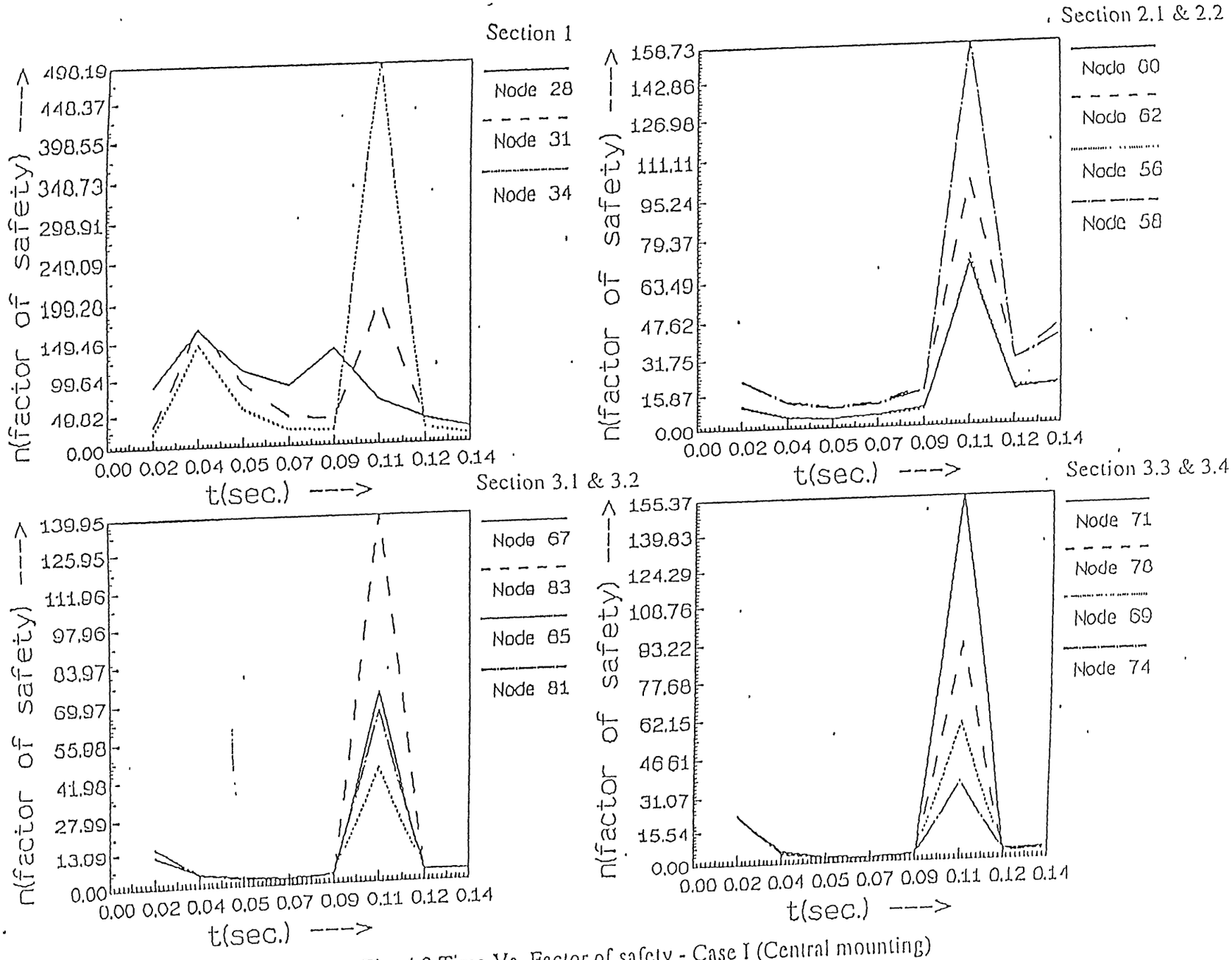

Fig. 4.2 Time Vs. Factor of safety - Case I (Central mounting)

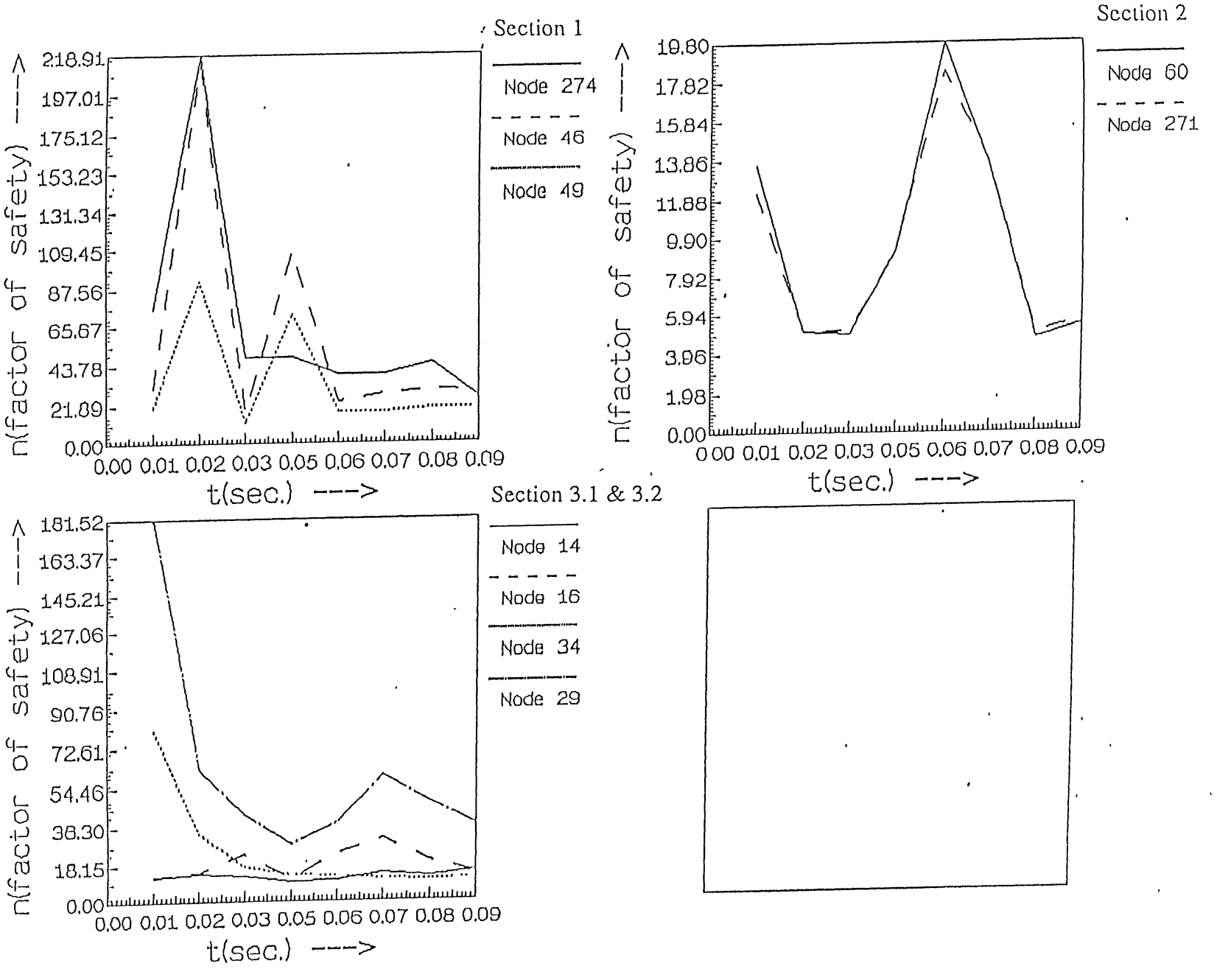

Fig. 4.3 Time Vs. Factor of safety - Case II (Side mounting)

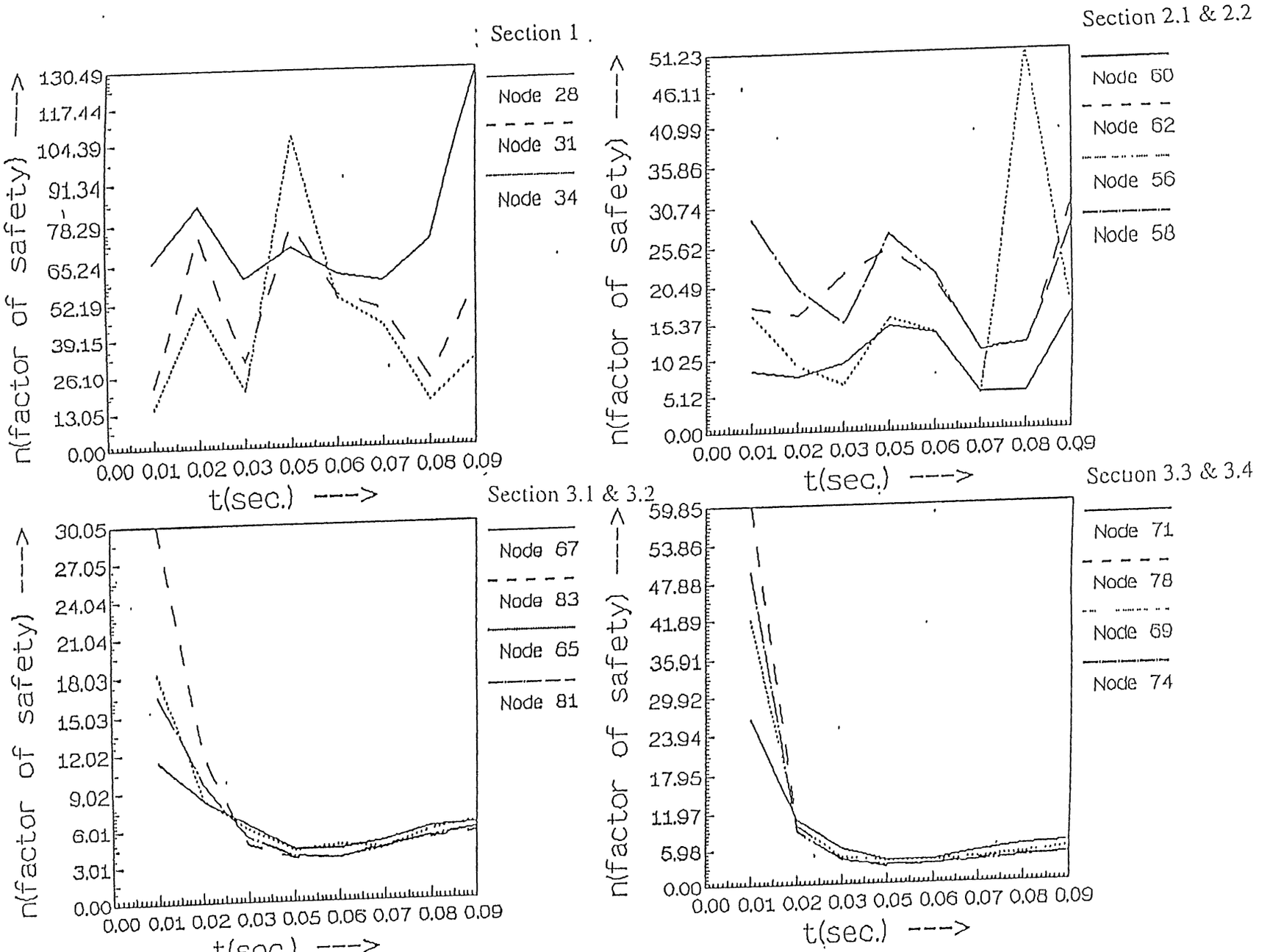
Section 1
Node 28
Node 31
Node 34
n(factor of safety) --->
130.49
117.44
104.39
91.34
78.29
65.24
52.19
39.15
26.10
13.05
0.00
0.00 0.01 0.02 0.03 0.05 0.06 0.07 0.08 0.09
t(sec.) --->
Section 2.1 & 2.2
Node 60
Node 62
Node 56
Node 58
n(factor of safety) --->
51.23
46.11
40.99
35.86
30.74
25.62
20.49
15.37
10.25
5.12
0.00
0.00 0.01 0.02 0.03 0.05 0.06 0.07 0.08 0.09
t(sec.) --->
Section 3.1 & 3.2
Node 67
Node 83
Node 65
Node 81
n(factor of safety) --->
30.05
27.05
24.04
21.04
18.03
15.03
12.02
9.02
6.01
3.01
0.00
0.00 0.01 0.02 0.03 0.05 0.06 0.07 0.08 0.09
t(sec.) --->
Section 3.3 & 3.4
Node 71
Node 78
Node 69
Node 74
n(factor of safety) --->
59.85
53.86
47.88
41.89
35.91
29.92
23.94
17.95
11.97
5.98
0.00
0.00 0.01 0.02 0.03 0.05 0.06 0.07 0.08 0.09
t(sec.) --->
Fig. 4.4 Time Vs. Factor of safety - Case II (Central mounting)

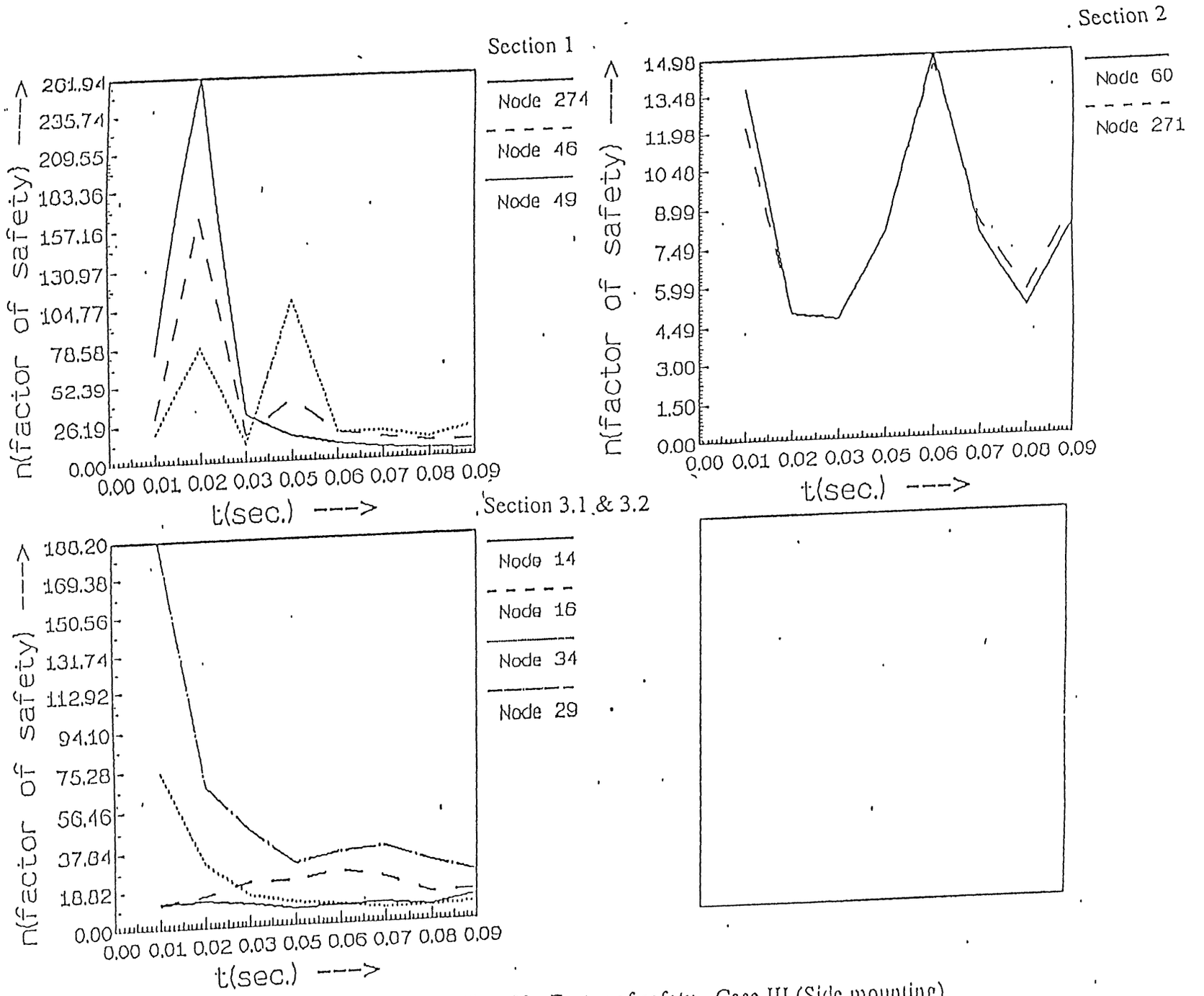

Fig. 4.5 Time Vs. Factor of safety - Case III (Side mounting)

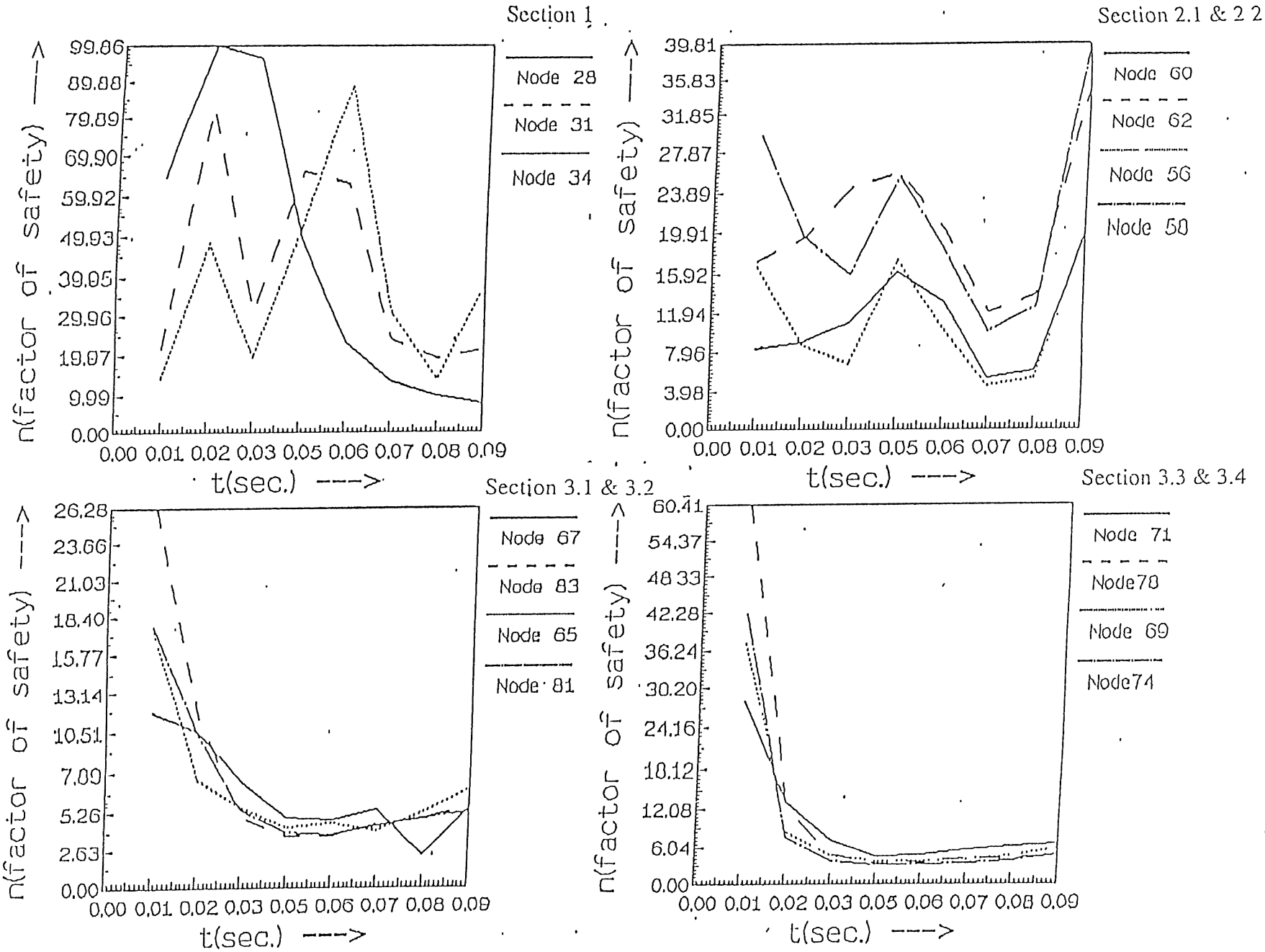

Fig. 4.6 Time Vs. Factor of safety - Case III (Central mounting)

3.1 and at node 34 for section 3.2. For the same case maximum shearing stress for the Central mounting frame occurs at node 34 for section 1, at nodes 60 and node 56 for sections 2.1 and 2.2 respectively, at nodes 83 and 81 for sections 3.1 and 3.2 respectively, and at node 78 and node 74 for sections 3.3 and 3.4 respectively. Except for section 2 maximum shearing stress occurs at different points in space in both the frames for similar sections. Value of maximum shearing stress is quiet high for sections 3.3 and 3.4 in the Central mounting frame which makes it a weak point for failure. The similar section is not present in the Side mounting frame. Fig. 4.2 also shows that factor of safety remains very low for sections 3.1 to 3.4 of Central mounting frame for most of the loading duration.

For Case II when the vehicle is running at 40 km./hr. in the fourth gear and its front wheel goes into a ditch of half sine wave of 2 m wavelength and 150 mm amplitude, maximum shearing stress for Side mounting frame occurs at node 49 for section 1, at node 60 for section 2, at node 14 for section 3.1 and at node 34 for section 3.2. For the same condition maximum shearing stress for the central mounting frame occurs at node 34 for section 1, at nodes 60 and 56 for sections 2.1 and 2.2 respectively, at nodes 83 and 81 for sections 3.1 and 3.2 respectively, and at nodes 78 and 74 for sections 3.3 and 3.4 respectively. In this case also the location of the maximum shearing stress points are same in space as is in the previous case, for section 2 and section 3 of both the models. Fig. 4.4 once again shows that section 3.3 and section 3.4 have lower factor of safety for most of the loading duration and are poor sections.

For Case III when the vehicle is running at 40 km./hr. in the fourth gear and its both rear wheels go into a ditch of half sine wave of 2 m wavelength and 150 mm amplitude, maximum shearing stresses for the Side mounting frame occurs at node 274 for section 1, at node 60 for section 2, at node 14 for section 3.1 and at node 34 for section 3.2. For the same conditions for the Central mounting frame maximum shearing stresses occurs at node 28 for section 1, at nodes 60 and node 56 for sections 2.1 and 2.2 respectively, at nodes 78 and 74 for sections 3.3 and 3.4 respectively. Once again in this case also for section 2 and section 3 maximum shearing stress points are located at the same place in space as is in the previous two cases, for both the two models. Again sections 3.1 to 3.4 of the Central mounting frame have the larger maximum shearing stress and sections 3.3 and 3.4 have the largest maximum shearing stress values.

From the above results it can be concluded that in both the models section 1 has the lowest stress developed. Section 1 and section 2 in both the models develop similar stress values for all the three cases. But section 3 in the Central mounting frame invariably has higher stress values in comparison to section 3 for the Side mounting frame. Sections 3.3 and 3.4 of the Central mounting frame are the weakest sections . Analysis shows that inspite of the Central mounting being a more balanced frame and engine being mounted in the middle of the frame , is a weaker frame due to sections 3.3 and 3.4. Similar sections are not present in the Side mounting frame. This can be attributed to the fact that the diameter of the load carrying tube has been reduced and the channel section has been replaced by tubural section in the Central mounting frame. This change reduces the area moment of inertia of load carrying member and hence increases the stresses developed in it.

CHAPTER - 5

EXPERIMENTAL VERIFICATION

5.1 THEORY OF STRAIN GAGE

The electrical resistance strain gage is basically a piece of very thin foil of fine wire Fig. 5.1 which exhibits a change in resistance proportional to the mechanical strain imposed on it. In order to handle such a delicate filament, it is either mounted or bonded to some type of carrier material and is known as the bonded strain gage. The strain gage is used universally in the experimental determination of stresses. The relation ship between resistance change and strain in the foil or wire used in strain gage construction can be expressed as:

$$\frac{\Delta L}{L} = \frac{\Delta R}{k * R}$$

or

$$k = \frac{\Delta R / R}{\Delta L / L} \qquad (5.1)$$

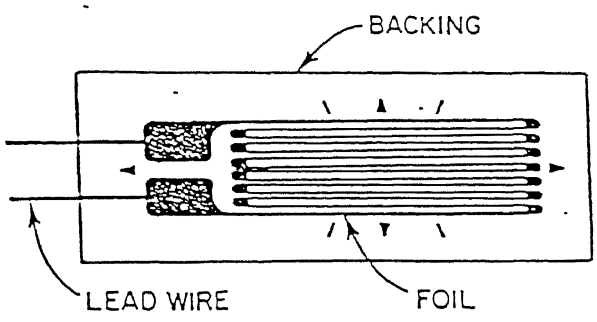

Fig. 5.1 Typical construction of a foil strain gage

where k is defined as the gage factor of the foil or wire, ΔR is the resistance change due to strain , R is the initial resistance, ΔL is the change in length, L is the original length of the wire or foil. and $\Delta L/L$ is the unit strain to which the wire or foil is subjected.

5.2 DETAILS OF BRIDGE CIRCUIT

The bridge circuit converts the change in resistance of the strain gauges bonded to the chassis frame into a potential difference. This potential difference is in turn, recorded on the oscilloscope. Fig. 5.2 shows the configuration of the bridge circuit used in this study. R_1 ,R_2 , R_3 and R_4 are four strain gauges each having a resistance value of $120 \pm 0.3\ \Omega$. R_1 represent the strain gauges bonded to the chassis frame. R_2 ,R_3 and R_4 are the dummy gauges. These dummy strain gauges are bonded on a steel plate which acts as a heat sink to the heat generated in the coils of the strain gauge when current flows through it. The bridge circuit is balanced to give zero voltage output for no change in resistance of the active strain gauges. This is done by connecting a 1.0 Ω resistance in series and two variable resistors (1.0 MΩ and 1.0 kΩ) parallel to one of the dummy strain gauges (R_2 in the shown circuit). To calibrate the bridge circuit a calibration resistance R_c is connected parallel to the active gauge through a switch (K). The value of the calibration resistance is 47.0 kΩ. The equation involving the calibration of the bridge circuit are as follows:

For a balanced bridge circuit the output voltage (Δe) is given by:

$$\frac{\Delta e}{E} = \frac{R_1 - R_2}{(R_1 + R_2)^2}\left(\frac{\Delta R_1}{R_1} - \frac{\Delta R_2}{R_2} + \frac{\Delta R_3}{R_3} - \frac{\Delta R_4}{R_4}\right) \qquad (5.2)$$

where E is the input voltage. It can be seen from the equation that similar (both positive or both negative) changes in resistance of opposite arms of the bridge circuit are added up and dissimilar (one positive and other negative) changes are canceled out.

The relation between the strain in the strain gauge and corresponding change in its resistance is governed by the Eqn. (5.1). Which is:

$$G.F. = \frac{\Delta R/R}{\Delta L/L}$$

$$\frac{\Delta L}{L} = \frac{\Delta R/R}{G.F.}$$

The change in resistance of the arm CD after connecting R_c is given by

$$\Delta R = R - \left(\frac{R * R_c}{R + R_c}\right)$$

leading to

R_1 : Active gage

R_2, R_3, R_4 : Dummy gages

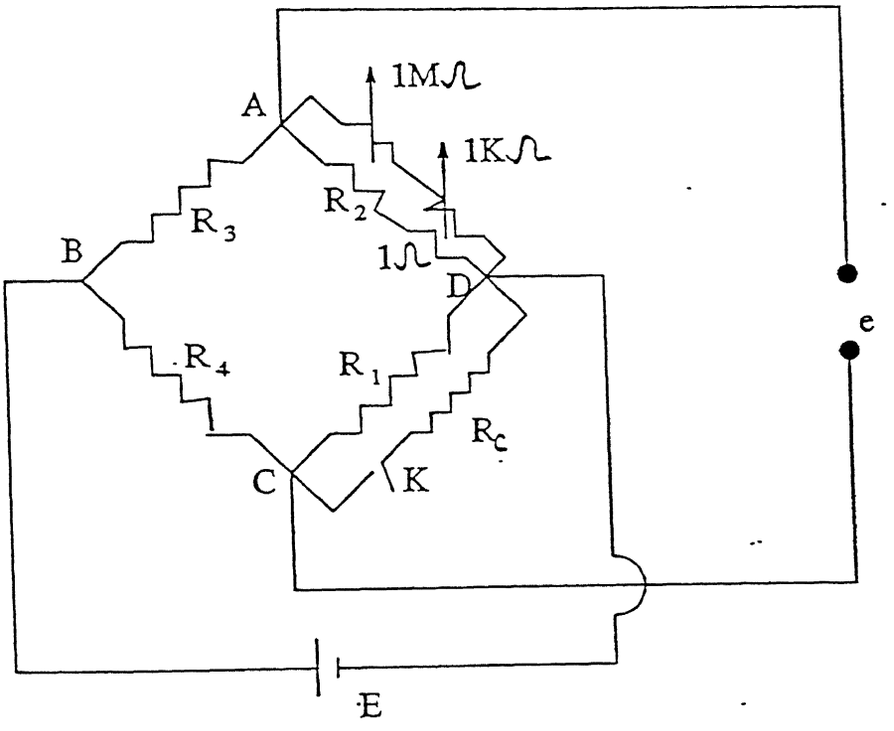

Fig. 5.2 Bridge circuit

$$\frac{\Delta R}{R} = \frac{R}{R + R_c} \tag{5.3}$$

corresponding to this change in resistance a voltage difference (calibration voltage, V_c) will occur between terminals A and C. This resistance change will also correspond to the strain in the strain gauge. From Eqns. (5.1) and (5.3) this strain will be:

$$\varepsilon_c = \frac{\Delta L}{L} = \frac{R}{(R + R_c) * G.F.} \tag{5.4}$$

The strain value ε_c will thus correspond to the calibration voltage, V_c.. By the linearity of the relation (Eqns. (4.1) and (4.2)) between voltage drop across AC strain in the strain gauges bonded to the frame, the strain in the frame corresponding to a voltage V recorded on the oscilloscope can be given as:

$$\varepsilon = \frac{\varepsilon_c}{V_c} V \tag{5.5}$$

5.3 OSCILLOSCOPE

1604 Digital storage oscilloscope has been used for experimental work. It can be operated in storage or non-storage modes as required. Two complete traces can be stored for future use and

four complete front panel control setup. With the optional battery backup facility, these can be retained even when it is switched off. Its input sensitivity is 500μV to 10V/div. This oscilloscope is provided with differential input facility. It has a band width of 3 MHz which means it can record signals up to 3 MHz frequency.

5.4) DETERMINATION OF PRINCIPAL STRAIN AND ITS DIRECTION:

For doing the verification of the models developed for NISA for doing analytical analysis, experiments have been performed on the chassis. Strain gauge has been put in the maximum absolute principal stress direction to measure the strain . This experimental value of strain has been compared with the theoretical value of strain given by theoretical analysis. Theoretically strain has been calculated from the following formulae:

$$\varepsilon_1 = \frac{1}{E}[\sigma_1 - \frac{1}{\nu}(\sigma_2 + \sigma_3)] \qquad (5.6)$$

Where,

ε_1 : Principal strain at a point

σ_1 , σ_2 , σ_3 : Three principal stresses acting on three mutually perpendicular planes at a point

ν: Poisson's ratio

E: Young's modulus

For determining the principal strain direction following theory has been developed:

From 3-D beam bending theory stress tensor is given as:

$$\begin{bmatrix} S_{xx}' & S_{xy}' & S_{xz}' \\ S_{xy}' & 0 & 0 \\ S_{xz}' & 0 & 0 \end{bmatrix} \tag{5.7}$$

and from torsional theory stress tensor is given as:

$$\begin{bmatrix} 0 & S_{xy}'' & S_{xz}'' \\ S_{xy}'' & 0 & 0 \\ S_{xz}'' & 0 & 0 \end{bmatrix} \tag{5.8}$$

3-D beam element in NISA incorporates both the bending and the torsion. Since element of the stress tensors can be added up to combine the effect of bending and torsion hence for 3-D beam element after adding Eqn.(5.7) and Eqn.(5.8) we get the stress tensor as:

$$[\sigma] = \begin{bmatrix} S_{xx} & S_{xy} & S_{xz} \\ S_{xy} & 0 & 0 \\ S_{xz} & 0 & 0 \end{bmatrix} \tag{5.9}$$

NISA gives all the elements of Eqn.(5.9), principal stresses and maximum shear stress in the output. Since the chassis is made of isotropic material (no directional property) the direction of the principal strains and principal stress will coincide. To calculate principal strain direction let us

assume that there is a plane **n** with direction cosines n_x , n_y and n_z on which the stress is wholly normal. Then we have:

$$\mathbf{T} = \sigma \mathbf{n} \tag{5.10}$$

The components of this along the x, y and z axes are:

$$T_x = \sigma n_x , \; T_y = \sigma n_y \text{ and } T_z = \sigma n_z \tag{5.11}$$

Stress tensor Eqn.(5.9) can also be written as:

$$S_{xx} n_x + S_{xy} n_y + S_{xz} n_z = T_x \tag{5.12.1}$$

$$S_{xy} n_x = T_y \tag{5.12.2}$$

$$S_{xz} n_x = T_z \tag{5.12.3}$$

from Eqn. (5.11) and Eqn. (5.12) we get:

$$n_y = \frac{S_{xy}}{\sigma} n_x \tag{5.13.1}$$

$$n_z = \frac{S_{xz}}{\sigma} n_x \tag{5.13.2}$$

We also know that

$$n_x^2 + n_y^2 + n_z^2 = 1 \tag{5.14}$$

on solving Eqn. (5.12) and Eqn. (5.13)

$$n_x^2 = \frac{1}{1+(\frac{S_{xy}}{\sigma})^2 + (\frac{S_{xz}}{\sigma})^2}$$

$$\therefore \quad n_x = \frac{1}{\sqrt{1+(\frac{S_{xy}}{\sigma})^2 + (\frac{S_{xz}}{\sigma})^2}} \tag{5.15.1}$$

$$n_y = \frac{S_{xy}}{\sigma\sqrt{1+(\frac{S_{xy}}{\sigma})^2 + (\frac{S_{xz}}{\sigma})^2}} \tag{5.15.2}$$

$$n_{zz} = \frac{S_{xz}}{\sigma\sqrt{1+(\frac{S_{xy}}{\sigma})^2 + (\frac{S_{xz}}{\sigma})^2}} \tag{5.15.3}$$

5.5 EXPERIMENTAL SETUP

Fig. 5.3 shows the schematic diagram and Fig. 5.5 shows the instrumentation for the complete experimental setup. Strain gage is pasted, Fig. 5.4, on the chassis at the critical points in the

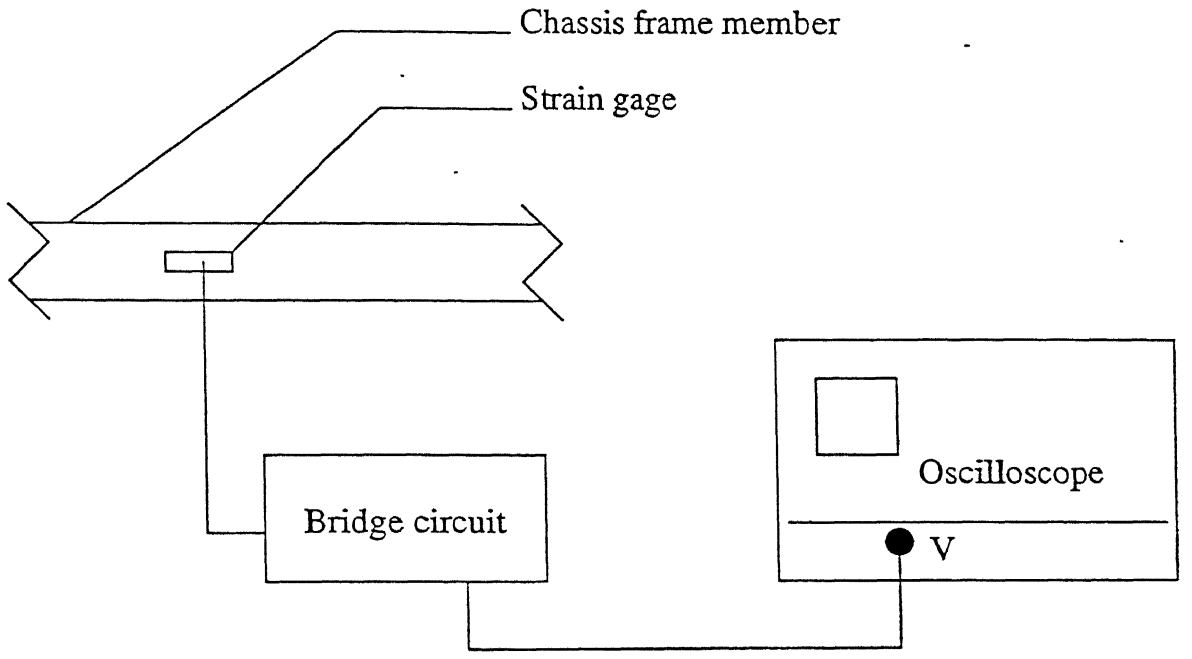

Fig. 5.3 Schematic diagram of experimental setup

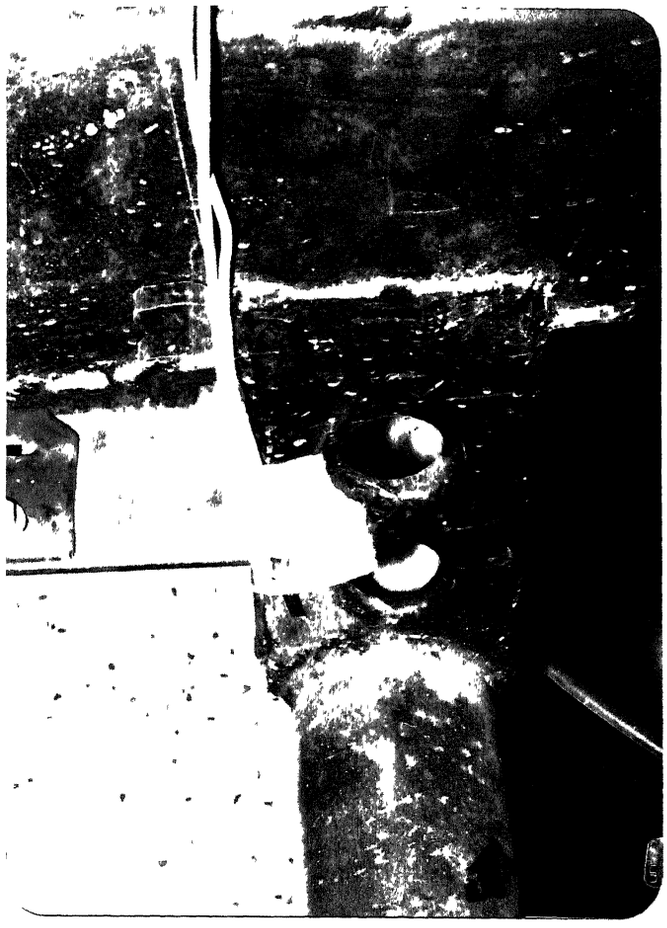

Fig. 5.4 Strain gage pasted on chassis member

Fig. 5.5 Oscilloscope with bridge circuit box

principal strain direction. It is connected to the bridge circuit through long coaxial wire. Bridge circuit gives the output to the oscilloscope.

5.6 RESULTS

Experiments has been performed for Case I i.e. for the condition when engine is idling. Table 5.1 and table 5.2 shows the expected theoretical maximum principal strain and the experimental principal strain values for selected nodes . for which experiments has been performed.

Maximum error in the expected value and experimental value is 94.7 %. Error varies from 8 % to 94.7 %. This error can be attributed to the simplifications made in the computer modeling due . to various reasons e.g. inability of the package to model the engine, power transmission system, tyres, non availability of the data for unbalanced engine forces, shock absorbers, complications involved in modeling for welded plates, distribution of load etc.. Error can also be attributed to the fact that experimental values has been taken when the steady state condition has been reached where as for doing computer modeling because of non availability of the steady state boundary condition data simplified boundary conditions have been applied.

Since various simplifications are done to do the computer modeling it is expected that the theoretical strain values will be more than the experimental strain values, which is verified by the principal strain values in the table 5.1 and table 5.2. With the limitation imposed for doing the

Node no.	Theoretical strain value	Experimental strain value	% Error
270	9.79e-4	1.989e-4	79.7
14	3.44e-4	0.37e-4	89

Table no. 5.1 Comparison of principal strains (Side mounting)

Node no.	Theoretical strain value	Experimental strain value	% Error
62	2.46e-4	0.54e-4	78
65	8.68e-4	0.46e-4	94.7
78	11.5e-4	10.625e-4	8

Table no. 5.2 Comparison of principal strains (Central mounting)

Node 270

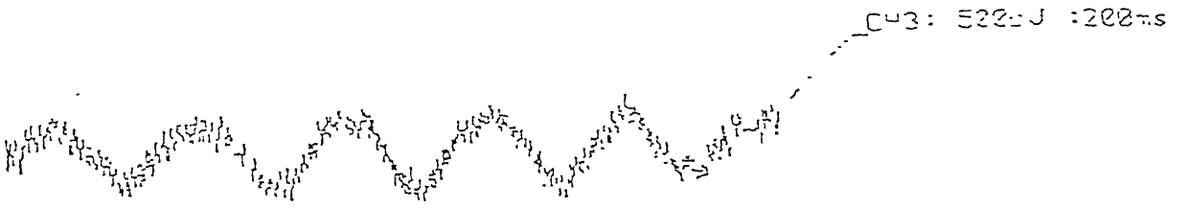

Node 14

Node 62

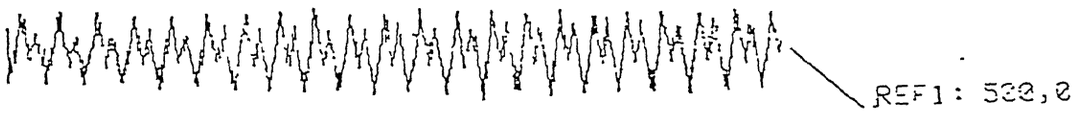

Node 65

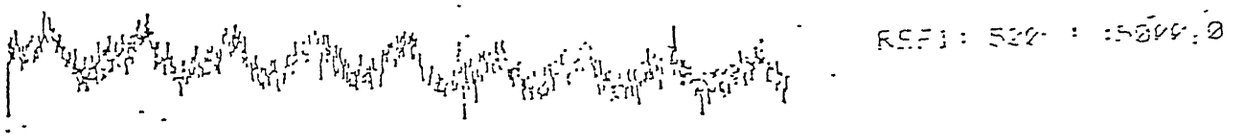

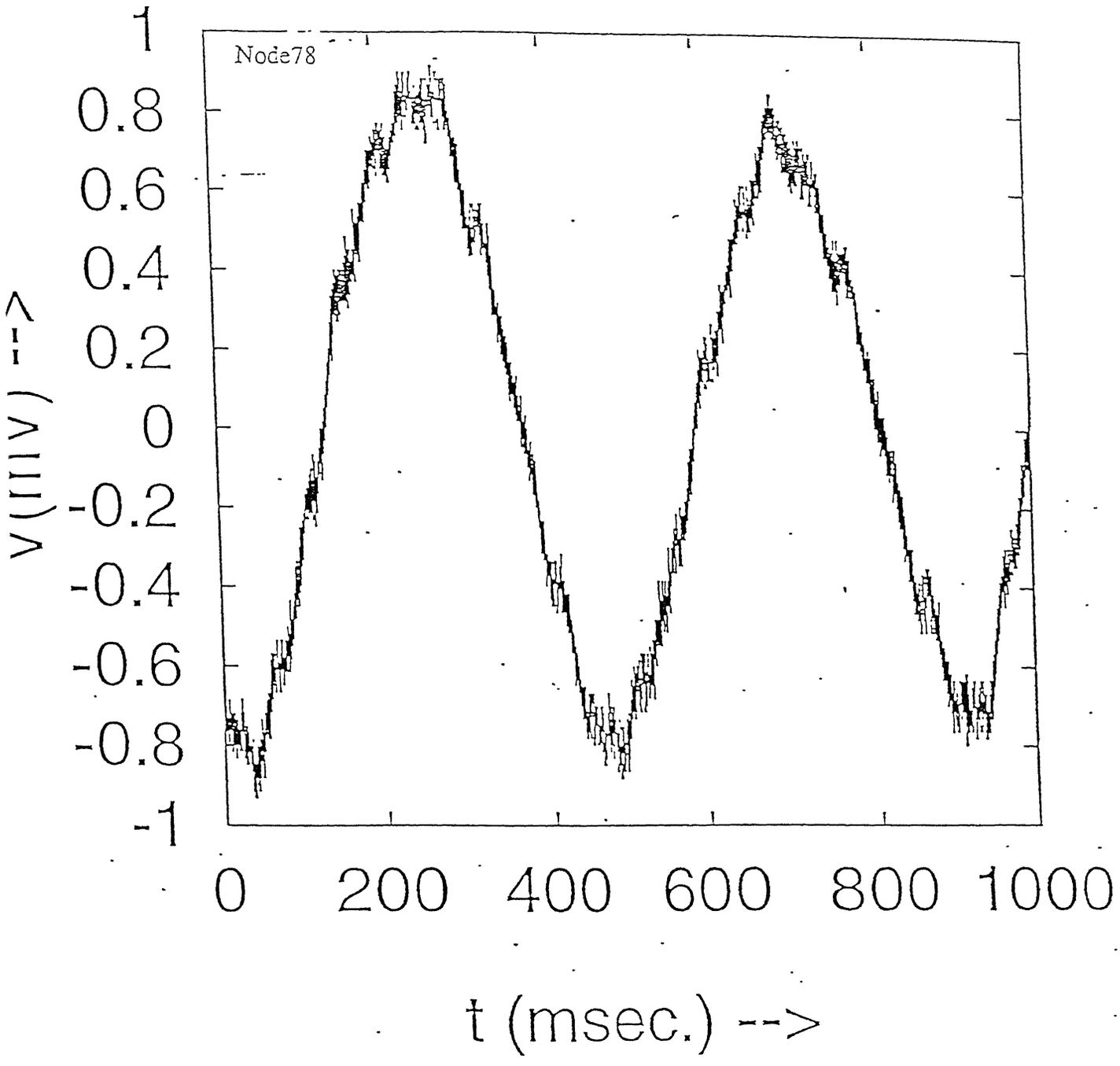

Fig. 5.6 Time Vs. Voltage outputs from oscilloscope

computer modeling it can be said that the errors are with in the acceptable norms and the computer model is fairly good for doing the required analysis for getting the qualitative solution.

CHAPTER - 6

CONCLUSION AND SCOPE FOR FUTURE WORK

In the present work computer modeling of the two chassis (with old and new design) acted upon by dynamic and static loads has been done. Finite element analysis of the two chassis models is done by using these computer models, to determine and compare stresses at critical sections under the loading conditions. These finite element analysis model and results have been verified by experimental stress analysis.

In this work various simplifications have been done due to various reasons. By using a better software package these simplifications can be reduced and stress predications can be done with greater accuracy. In the present work finer mesh can be generated and more points can be selected for finer stress variation analysis.

For doing experimental analysis only a few points have been selected. The number of points for doing experimental analysis can be increased. Experimental stress values can also be taken at different engine speeds. By using strain rosettes strain fields at various critical points can be found out and detailed experimental stress analysis can be done. For Case II and Case III theoretical results can be verified by using a pulsator to simulate the ditch boundary condition. Also vehicle can be run in the actual road conditions and by using on board instruments experiments can be performed for real conditions.

REFERENCES

1. Ali R. and Hedge J.L. "Static Analysis of a Light Truck Frame using the FEM", International conference on Vehicle structures, ME conference Publications, 1984.

2. Costin M. and Phipps D. "Racing and Sports car chassis design".

3. Joshi N. "A study and improvement in design of engine mount of three wheeler Vikram", M.Tech. thesis, Department of Mechanical Engineering, I.I.T.Kanpur, 1994.

4. Luckin P., Gasparyants G., Rodionov V. "Automobile Chassis - design and calculation", Mir Publications, Moscow, 1989.

5. Mahadevan K. and Reddy K.B. "Design Data Hand Book", CBS Publication and Distributors, Delhi, 1989.

6. NISA II, User's manual Vol. 1 and Vol. 2, 1994.

7. Punmia B.C., Ashok J. and Jain A. "Strength of Materials", Laxmi Publications, N. Delhi, 1992.

8. Sharman P.W. "The use of Dynamic Strain Recorders to Estimate the Fatigue life of a semi-trailer chassis", Stress, Vibration and Noise analysis in vehicles, 1975.

9. Srinath L.S. "Advanced Mechanics of Solids", Tata McGraw - Hill Publishing Company Limited, N. Delhi, 1994.

10. Weaver W. and Johnston P.R. "Structural Dynamics by Finite Elements", Prentice - Hall, Inc., New Jersey, 1987.

APPENDIX

```
dimension a(8),b(8)

a(1) = 0.01125
b(1) = 0.01755
sum1 = 0.01125
sum2 = 0.01755
do i = 1,7
 a(i+1) = a(i) + sum1
 b(i+1) = b(i) + sum2
enddo
open(unit = 10,file = 'cd81.in')
open(unit = 20,file = 'Node81')
x = 220000
do i = 1,8
read(10,*) y
s = x/y
write(20,*)a(i),s
write(20,*)b(i),s
enddo
stop
end
```